

Supplementary Information

The Regenerative Role of Biofilm in the Removal of Pesticides from Stormwater in Biochar-Amended Biofilters

Andrea C. Portmann¹, Gregory H. LeFevre², Rennosuke Hankawa¹, David Werner³, Christopher
P. Higgins^{1*}

¹Department of Civil & Environmental Engineering, Colorado School of Mines, Golden, Colorado 80401,
United States

²Department of Civil & Environmental Engineering and IIHR-Hydroscience & Engineering, University of
Iowa, Iowa City, IA 52242, United States

³School of Engineering, Newcastle University, Newcastle upon Tyne, NE1 7RU, United Kingdom

*** Corresponding author:**

Christopher Higgins, 720-984-2116, chiggins@mines.edu

Table of Contents

1. TOrCs Analysis	S2
2. Microbial Transformation Pathways	S4
3. Materials	S11
4. Batch Sorption Experiments	S13
5. Column Experiments	S17
6. Transformation Products & Suspect Screening	S20
7. Transport Modelling	S27

1. TOrCs Analysis

Table S1: Native and surrogate standard sources for investigated trace organic chemicals (TOrCs).

Compound Name	Abbreviation	Chemical Formula	CAS #	Analytical Standard Source	Spiking Standard Source
Atrazine	ATZ	C ₈ H ₁₄ ClN ₅	1912-24-9	Fluka, Pestanal®	TCI America, >97%
Desethyl-Atrazine	DEA	C ₆ H ₁₀ ClN ₅	6190-65-4	Sigma-Aldrich, Pestanal®	-
De(s)isopropyl-Atrazine	DIA	C ₅ H ₈ ClN ₅	1007-28-9	Sigma-Aldrich, Pestanal®	-
2-Hydroxy-Atrazine	OH-ATZ	C ₈ H ₁₅ N ₅ O	2163-68-0	Sigma-Aldrich, Pestanal®	-
Imidacloprid	IMI	C ₉ H ₁₀ ClN ₅ O ₂	138261-41-3	SPEX CertiPrep, Certified Reference Material	Sigma-Aldrich, Pestanal®
Desnitro-Imidacloprid	Desnitro-IMI	C ₉ H ₁₁ ClN ₄	127202-53-3	Sigma-Aldrich, Pestanal®	-
Imidacloprid-Urea	IMI-Urea	C ₉ H ₁₀ ClN ₃ O	120868-66-8	LGC Standards	-
Imidacloprid-Olefin	IMI-Olefin	C ₉ H ₈ ClN ₅ O ₂	115086-54-9	Toronto Research Chemicals	-
6-Chloronicotinic-Acid	6-CNA	C ₆ H ₄ ClNO ₂	5326-23-8	Toronto Research Chemicals	-
Clothianidin	CLO	C ₆ H ₈ ClN ₅ O ₂ S	210880-92-5	SPEX CertiPrep, Certified Reference Material	Sigma-Aldrich, Pestanal®
Atrazine-d ₅	ATZ-d ₅	C ₈ H ₉ 2H ₅ ClN ₅	163165-75-1	C/D/N Isotopes, 99% D	-
Imidacloprid-d ₄	IMI-d ₄	C ₉ 2H ₄ H ₆ ClN ₅ O ₂	1015855-75-0	C/D/N Isotopes, 99% D	-
Clothianidin-d ₃	CLO-d ₃	C ₆ 2H ₃ H ₅ ClN ₅ O ₂ S	1262776-24-8	C/D/N Isotopes, 98% D	-

Table S2: LC-QToF-MS parameters for target analytes including parent compounds, transformation products, and surrogates. Analysis was performed in ESI+ ionization mode. ⁺ Surrogate corrected spike recovery in synthetic stormwater. *Data not available due to late addition of TP to analyte list.

Compound name	Formula	LOQ [ug/L]	Spike recovery ⁺ [%]	Precursor Mass (Q1) [Da], [M+H]	Fragment Mass (Q3) [Da]	RT [min]	Fragments [Da], Literature	References
Atrazine	C8H14ClN5	0.005	80	216.10105	174.05390	6.07	174.2, 103.9	Ulrich et al. 2017
Imidacloprid	C9H10ClN5O2	0.005	75	256.05958	175.0977	5.51	209.0585, 175.0982	Pandey et al. 2009, Xie et al. 2011
Clothianidin	C6H8ClN5O2S	0.005 – 0.025	76	250.01600	169.05390	5.25	169.0, 131.9	Xie et al. 2011
Desethyl-Atrazine	C6H10ClN5	0.005	95	188.06975	146.0228, 104.0010	5.19	146.2, 104.1	Ulrich et al. 2017
Desisopropyl-Atrazine	C5H8ClN5	0.005	96	174.05410	146.0228, 132.0322	4.67	146.2, 132.3	
Hydroxy-Atrazine	C8H15N5O	0.005	111	198.13494	156.0878, 86.0348	4.74	156.1, 85.9	
Desnitro-/guanidine-Imidacloprid	C9H11ClN4	0.005	91	211.07450	126.0105, 90.0335	4.55	126, 90	Raina-Fulton & Behdarvandan, 2016
Imidacloprid-Urea	C9H10ClN3O	0.005	83	212.05852	128.0256, 99.0551	5.15	128, 99	
Imidacloprid-Olefin	C9H8ClN5O2	0.005	97	254.04393	236.0340, 171.0667	5.11	236, 171	
6-Chloronicotinic Acid*	C6H4ClNO2	0.05	-	158.00033	122.02320, 78.0338	4.99	122.0, 78.0	Berset et al. 2017; Hao et al. 2016
Atrazine-d5	C8H9 2H5ClN5	-	-	221.13243	-	6.07	179.2	Ulrich et al. 2017
Imidacloprid-d4	C9 2H4H6ClN5O2	-	-	260.08469	-	5.51	213.1, 179.2	Xie et al. 2011
Clothianidin-d3	C6 2H3H5ClN5O2S	-	-	253.03483	-	5.25	172, 132	Raina-Fulton & Behdarvandan, 2016

LC Conditions

HPLC eluents, analysis blanks and double blanks, and sample dilutions (column effluents) were prepared using Optima® LC/MS-grade water and methanol and HPLC-grade acetonitrile (Fisher Scientific). The aqueous mobile phase (A) was 1 mM ammonium formate (Sigma-Aldrich) and 0.1% formic acid (Fluka) in Optima® LC/MS-grade water and the organic mobile phase (B) was 100% HPLC-grade acetonitrile. A flowrate of 0.6 mL/min was employed and the temperature of the column oven was held at 40°C. The HPLC gradient started out at 5% B, increased to 95% B within 5 min, stayed constant at this level for 5.5 min, until it quickly receded to 5% B for another 7.5 min to establish equilibrium conditions. Select samples and calibration standards for analysis

of 6-CNA were acidified with formic acid (0.225% final concentration in sample vial) to avoid peak splitting issues during liquid chromatography.

MS Parameters

Precursor ion data (TOF MS) was collected for m/z 50-1000 Da for 2271 cycles with a total scan time of 0.476 s and an accumulation time of 0.1 s, with ion spray voltage set at 5500 V and temperature set to 500 °C. The ion source gas 1 and 2, curtain gas, and collision (CAD) gas were set to 50 psi, 40 psi, 25 psi, and 10 psi, respectively. The collision energy (CE) was set to 5 V and the declustering potential (DP) to 50 V, each with no spread. Product ion (TOF MS/MS) scanning was conducted for m/z 50-1000 Da. The accumulation time for each SWATH window was 0.05 s and the CE was set to 30 V with 20 V spread, whereas the DP was kept at 50 V without spread. The instrument was mass calibrated every five injections using SCIEX ESI Positive Calibration Solution.

2. Microbial Transformation Pathways

Using the EAWAG Biocatalysis/Biodegradation Database and Pathway Prediction System (EAWAG-BBD/PPS; <http://eawag-bbd.ethz.ch/index.html>) and microbial transformation data available in literature, we compiled an extracted ion chromatogram (XIC) list of known and suspected TPs of atrazine, imidacloprid, and clothianidin (Table S3). The most widely identified transformation products were then used to develop common microbial transformation pathways for each of the three compounds, as shown in Figures S1-S3.

Table S3: Extracted ion chromatogram (XIC) list of microbial transformation products of atrazine, imidacloprid, and clothianidin.

Organic Contaminant	Formula	Exact Mass	Source
ATRAZINE	C8H14CIN5	215.093781	
Hydroxyatrazine	C8H15N5O	197.12766	EAWAG Pathway Predictor; Mudhoo & Garg, 2011; Singh et al. 2018; Fang et al. 2014; Kolekar et al. 2014; Sagarkar et al. 2013
Desethylatrazine	C6H10CIN5	187.062473	EAWAG Pathway Predictor; Mudhoo & Garg, 2011; Singh et al. 2018; Fang et al. 2014; Kolekar et al. 2014; Singh & Cameotra, 2014; Sagarkar et al. 2013
Deisopropylatrazine	C5H8CIN5	173.046823	EAWAG Pathway Predictor; Mudhoo & Garg, 2011; Singh et al. 2018; Fang et al. 2014; Kolekar et al. 2014; Singh & Cameotra, 2014; Sagarkar et al. 2013
Acetone	C3H6O	58.041865	EAWAG Pathway Predictor
N-Isopropylammelide	C6H10N4O2	170.080376	EAWAG Pathway Predictor; Singh et al. 2018; Fang et al. 2014; Kolekar et al. 2014; Sagarkar et al. 2013
2,4-Dihydroxy-6-(N'-ethyl)amino-1,3,5-triazine / N-Ethylammelide	C5H8N4O2	156.064726	EAWAG Pathway Predictor; Singh et al. 2018; Fang et al. 2014; Sagarkar et al. 2013
Isopropylamine	C3H9N	59.073499	EAWAG Pathway Predictor
	C6H11N5O	169.09636	EAWAG Pathway Predictor
Deisopropylhydroxyatrazine	C5H9N5O	155.08071	EAWAG Pathway Predictor; Singh et al. 2018; Fang et al. 2014; Kolekar et al. 2014; Sagarkar et al. 2013
	C6H9CIN4O	188.046489	EAWAG Pathway Predictor
Deisopropyldeethylatrazine / Didealkylatrazine	C3H4CIN5	145.015523	EAWAG Pathway Predictor; Mudhoo & Garg, 2011; Singh et al. 2018; Fang et al. 2014; Kolekar et al. 2014; Singh & Cameotra, 2014; Sagarkar et al. 2013
	C5H7CIN4O	174.030839	EAWAG Pathway Predictor
Cyanuric acid	C3H3N3O3	129.017442	EAWAG Pathway Predictor; Singh et al. 2018; Fang et al. 2014; Sagarkar et al. 2013
2,4-Dihydroxy-6-amino-1,3,5-triazine / Ammelide	C3H4N4O2	128.033426	EAWAG Pathway Predictor; Singh et al. 2018; Fang et al. 2014; Singh & Cameotra, 2014; Sagarkar et al. 2013
2-Hydroxy-4,6-diamino-1,3,5-triazine	C3H5N5O	127.04941	EAWAG Pathway Predictor
	C3H2CIN3O2	146.983555	EAWAG Pathway Predictor
2-Chloro-4-hydroxy-6-amino-1,3,5-triazine	C3H3CIN4O	145.999539	EAWAG Pathway Predictor; Singh et al. 2018; Fang et al. 2014; Sagarkar et al. 2013
Biuret	C2H5N3O2	103.038177	Fang et al. 2014; Sagarkar et al. 2013
Allophanate	C2H4N2O3	104.022193	Sagarkar et al. 2013

IMIDACLOPRID	C9H10CIN5O2	255.052303	EAWAG Pathway Predictor; Hussain et al. 2016; Pandey et al. 2009; Sharma et al. 2015
Imidacloprid-Urea	C9H10CIN3O	211.05124	EAWAG Pathway Predictor
Imidazolidinone	C3H6N2O	86.048013	EAWAG Pathway Predictor
	C6H4CINO	140.998142	EAWAG Pathway Predictor
	C9H11CIN3O2	228.05398	EAWAG Pathway Predictor
	C3H7N2O2	103.050753	EAWAG Pathway Predictor; Hussain et al. 2016; Sharma et al. 2014; Sharma et al. 2015
(Base form of) 6-Chloronicotinic Acid	C6H3CINO2	155.985232	EAWAG Pathway Predictor
	C6H7CIN2	142.029776	EAWAG Pathway Predictor
	C3H4NO3	102.019119	EAWAG Pathway Predictor
	C8H12CIN3	185.071975	EAWAG Pathway Predictor; Hussain et al. 2016; Pandey et al. 2009; Sharma et al. 2015
5-Hydroxyimidacloprid	C9H10CIN5O3	271.047218	Hussain et al. 2016; Sharma et al. 2014
Imidacloprid-Olefin	C9H8CIN5O2	253.036653	Hussain et al. 2016
Nitrosoguanidine metabolite / Nitrosimine imidacloprid	C9H10CIN5O	239.057388	Hussain et al. 2016; Pandey et al. 2009; Sharma et al. 2014
Aminoguanidine metabolite	C9H12CIN5	225.078123	Hussain et al. 2016; Pandey et al. 2009
Desnitro/guanidine metabolite / Imidacloprid NTG	C9H11CIN4	210.067224	Hussain et al. 2016; Pandey et al. 2009; Sharma et al. 2014; Sharma et al. 2015
6-Hydroxynicotinic acid	C6H5NO3	139.026944	Hussain et al. 2016
6-Oxo-1,4,5,6-tetrahydronicotinic acid	C6H7NO3	141.042594	Hussain et al. 2016
2-Formyl glutarate	C6H6O5	158.021525	Hussain et al. 2016
1-[(6-Chloropyridin-3-yl)methyl]imidazolidine-2,4-dione	C9H8CIN3O2	225.030505	Sharma et al. 2015
???	C9H10N4	174.090546	Sharma et al. 2015
2-Chloro-5-methylpyridine	C6H6CIN	127.018877	Sharma et al. 2015
CLOTHIANIDIN	C6H8CIN5O2S	249.008725	
1-[(2-Chloro-1,3-thiazol-5-yl)methyl]-3-nitrourea; CTNU	C5H5CIN4O3S	235.977091	EAWAG Pathway Predictor
	C4H5CIN2S	147.986198	EAWAG Pathway Predictor
	C5H4CIN2O2S	190.968203	EAWAG Pathway Predictor
	C5H5CIN4O4S	251.972006	EAWAG Pathway Predictor
	C4H2CINOS	146.954564	EAWAG Pathway Predictor
	C4H5CIN2OS	163.981113	EAWAG Pathway Predictor
	C5H4CIN2O3S	206.963117	EAWAG Pathway Predictor
	C5H5CIN4O5S	267.966921	EAWAG Pathway Predictor
	C4H2CINO2S	162.949479	EAWAG Pathway Predictor
	C4HCINO2S	161.941654	EAWAG Pathway Predictor
	C4H5CIN2O2S	179.976028	EAWAG Pathway Predictor

N-(2-chlorothiazol-5-yl-methyl)-N'-methylurea; thiazolylmethylurea; TZMU; clothianidin-urea	C6H8CIN3OS	205.007662	Van der Velde-Koerts et al. 2011; Mori et al. 2017; Zhang et al. 2018
N-(2-chlorothiazol-5-yl-methyl)-N'-nitroguanidine; thiazolylnitroguanidine; TZNG	C5H6CIN5O2S	234.993075	Van der Velde-Koerts et al. 2011
N-methyl-N'-nitroguanidine; 1-methyl-2-nitroguanidine; MNG	C2H6N4O2	118.049076	Van der Velde-Koerts et al. 2011
Nitroguanidine; NTG	CH4N4O2	104.033426	Van der Velde-Koerts et al. 2011
3-Methyl-1-[(1,3-thiazol-5-yl)methyl]urea	C6H9N3OS	171.046634	Zhang et al. 2018

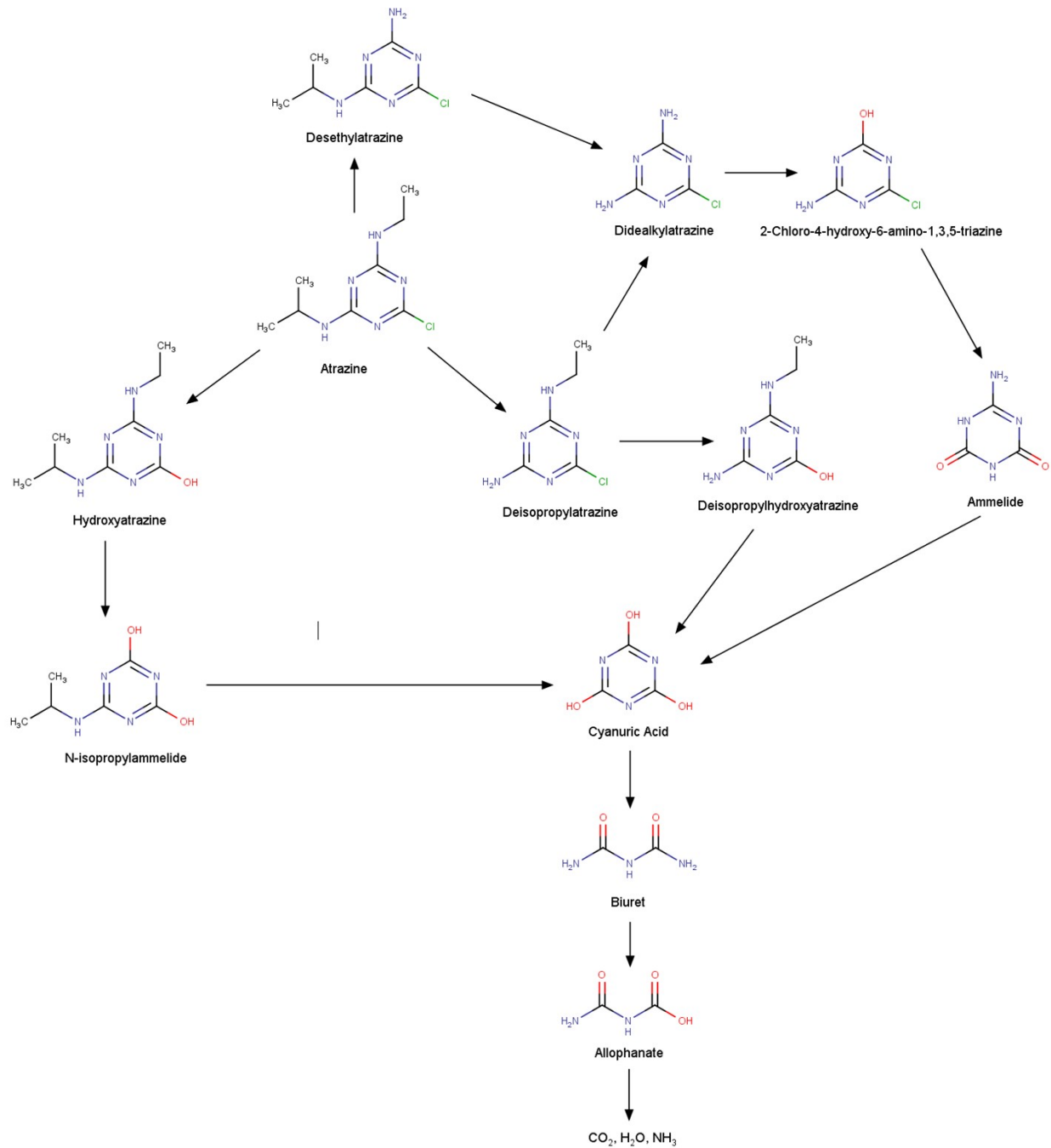


Figure S1: Literature-established major microbial transformation pathway for atrazine. Sources: Singh et al. 2018; Mudhoo & Garg, 2011; Fang et al. 2014; Kolekar et al. 2014; Singh & Cameotra, 2014; Sagarkar et al. 2013.

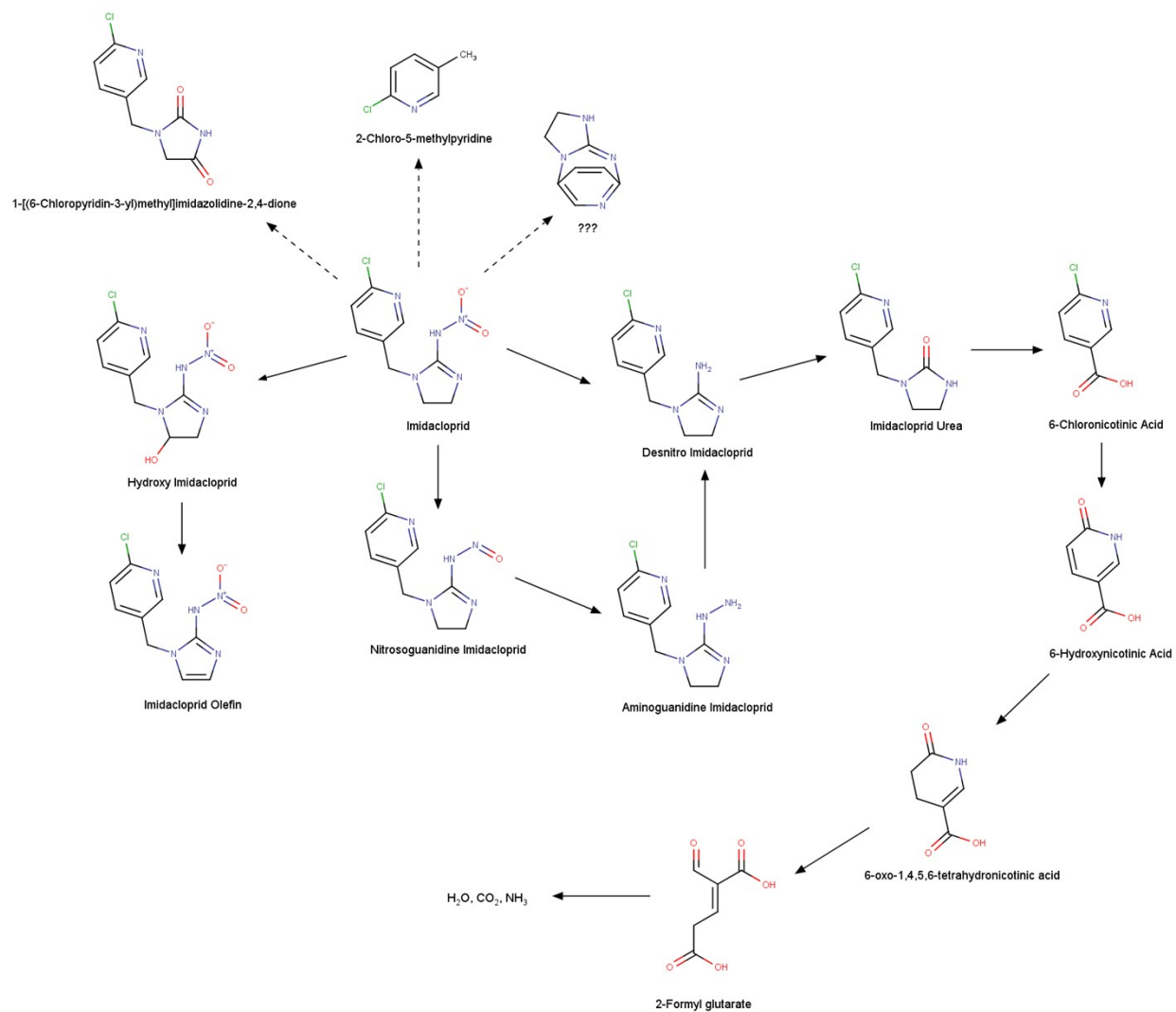


Figure S2: Literature-established major microbial transformation pathways for imidacloprid as indicated by literature sources. Sources: Hussain et al. 2016; Sharma et al. 2014; Pandey et al. 2009; Sharma et al. 2015.

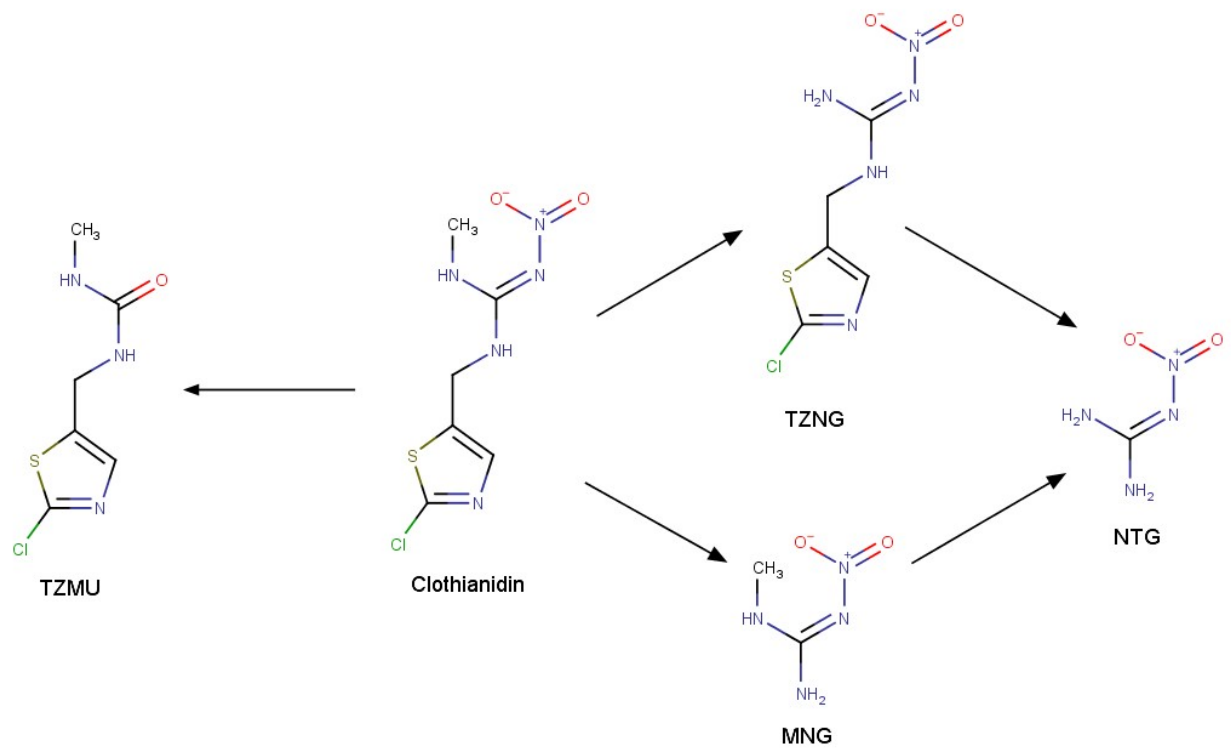


Figure S3: Literature-established major microbial transformation pathway for clothianidin. Sources: Van der Velde-Koerts et al. 2011.

3. Materials

Biochar Characterization

To characterize the physical properties of the biochar used, the Brunauer-Emmett-Teller specific surface area (BET SSA) and the total pore volume (PV) were measured using a Micromeritics Gemini V surface area and pore size analyzer (Norcross, GA). Total pore volume and pore size distributions for macropores (>50 nm) and mesopores (2-50 nm) were calculated from Barrett, Joyner, and Halenda (BJH) desorption isotherms. Estimation of micropore (<2 nm) volumes was based on t-Plot micropore volume measurements using the same instrument. Prior to measurement, sample masses were added to the analysis tubes (<0.1 g for pure biochar samples, >0.5 g for mixed sand-biochar samples) and degassed overnight at 100 °C at <50 mTorr. BET SSA measurements were acquired using 11 points, whereas BJH adsorption and desorption isotherms were measured using 40 points each. Detection limits for BET analysis were ~1 m²/g. t-Plot micropore volume measurements of aged sand-biochar samples were below the limit of detection due to the low mass percentages of biochar (0.5 wt%) in these samples.

DOC Extract Solutions (“DOC Teas”)

The DOC extract solutions (DOC teas) were prepared as follows: Five gallons of nearby creek water (Clear Creek, Golden, CO) were collected and grass and leaves from residential curbs and stormwater ditches and woody plant-based EcoGrow compost (A1 Organics; Eaton, CO) were added as DOC sources. The solution was incubated for three weeks at room temperature (18-20 °C) and shaken occasionally. The leachate was then centrifuged in small batches at 500 rpm and the supernatant was subsequently filtered employing a three-step membrane filtration process starting with 2.7 µm (Whatman, GF/D Glass Microfiber Filters), followed by 0.7 µm (Whatman, GF/F Glass Microfiber Filters), and finally a 0.45 µm filter (Supor-450, PALL). The filtered DOC

solution was distributed into separate 1L and 2L PYREX glass bottles, which were autoclaved for sterilization at 121 °C for 1.5 hours, and then refrigerated at 4°C.

During the total four months of column operation and influent preparation, we started with one bottle and as soon it was used up (typically within 2 weeks), we moved on to the next one. To avoid microbial contamination, respective DOC solution volumes were poured into separate beakers for use (extra volumes were discarded), and no pipet tips or similar were ever introduced into the glass storage bottles. The DOC concentration of each newly opened bottle was determined via TOC-L Laboratory Total Organic Carbon Analyzer to determine the correct volume to use for the influent preparation. Furthermore, DOC concentrations in the prepared influent were measured twice a week during the first seven weeks, and then weekly after that. Visual inspection of the solution in the clear glass bottles in addition to changes in smell (due to bacterial growth) were performed during each influent preparation.

4. Batch Sorption Experiments

Sorption Isotherms

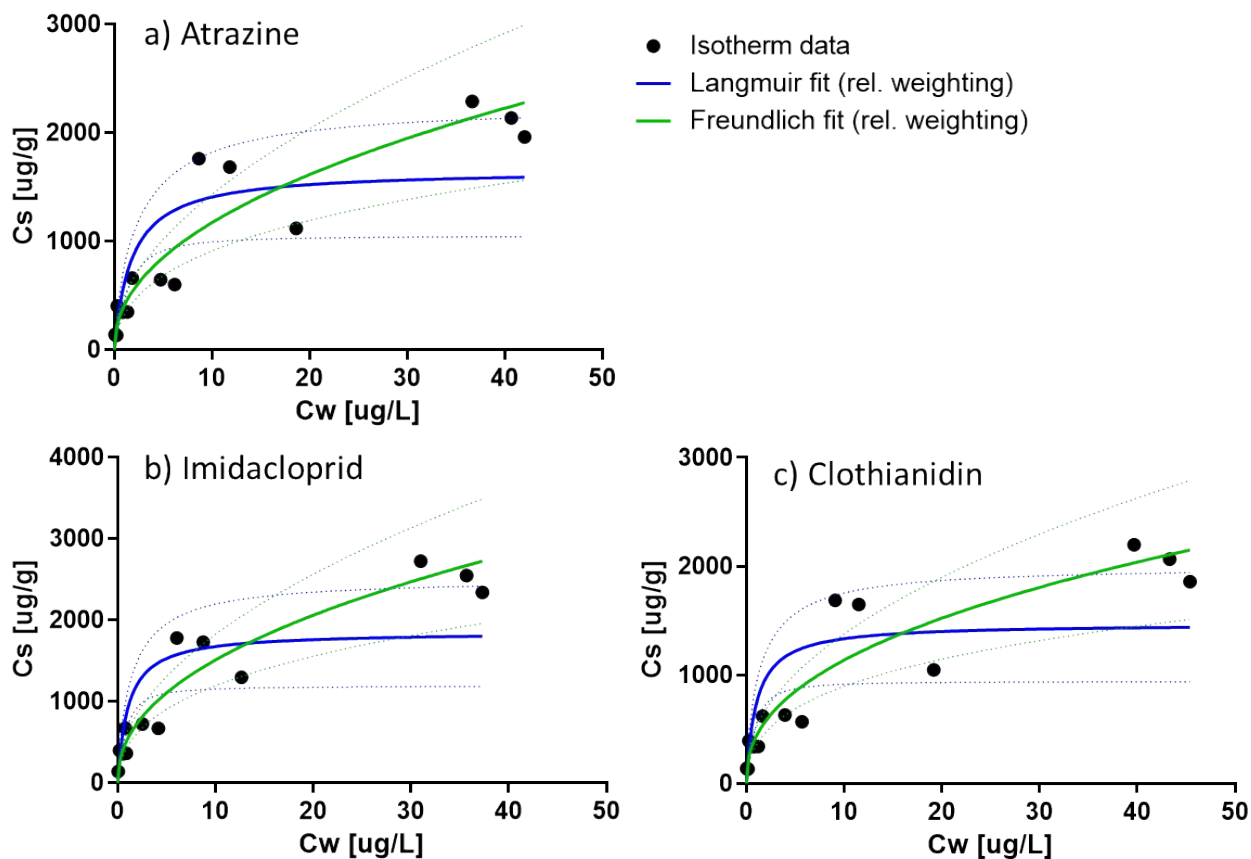


Figure S4: Solid lines represent best fits of the Freundlich and Langmuir equations to batch sorption isotherm data using non-linear regression and relative weighting ($1/Y^2$). Dotted lines represent the 95% confidence intervals of the fitted curves. The systematic error in the observed datapoints across all three pesticides was likely caused by uncertainties in dry biochar mass (due to its extremely light weight and hydrostatic behavior).

Table S4: Best-fit values for Freundlich and Langmuir parameters obtained in GraphPad Prism (version 9.1.1). AICc designates the Akaike's Information Criterion corrected for low sample size. Please note that the KF values are not significantly different from each other ($p=0.1261$), the same is true for the parameter n ($p=0.7542$; One-way ANOVA, $\alpha = 0.05$).

	Atrazine	Imidacloprid	Clothianidin
<i>Freundlich</i>			
K_F [(ug/g)/((ug/L)ⁿ)]	402.2	535.0	429.6
K _F 95% CI [(ug/g)/((ug/L) ⁿ)]	356.8 to 610.3	483.5 to 723.9	384.0 to 617.4
n [-]	0.4638	0.4495	0.4221
n 95% CI [-]	0.3546 to 0.5484	0.3612 to 0.5197	0.3312 to 0.4970
Weighted Sum of Squares (1/Y ²)	1.502	1.151	1.365
RMSE	0.3276	0.2867	0.3122
AICc	-26.33	-30.33	-27.78
AIC probability that the model is correct [%]	94.76	99.18	98.96
<i>Langmuir</i>			
Q_{max} [ug/g]	1658	1850	1472
Q _{max} 95% CI [ug/g]	1340 to 2722	1518 to 3097	1216 to 2532
KL [L/ug]	0.5590	0.9412	0.9614
KL 95% CI [L/ug]	0.3398 to 1.078	0.5664 to 1.676	0.5645 to 1.841
Weighted Sum of Squares (1/Y ²)	2.210	2.180	2.506
RMSE	0.3973	0.3946	0.4231
AICc	-20.54	-20.75	-18.66
AIC probability that the model is correct [%]	5.241	0.825	1.036

Kinetic Sorption Equilibrium

Table S5: Equilibrium K_d (\pm standard deviation) calculated from kinetic batch sorption data at timepoint $t=67$ days. It was concluded that sorption equilibrium had been established for all compounds since linear regression analysis between $t=29$ days and 67 days revealed that slopes did not significantly deviate from zero ($p \geq 0.7498$). Tukey's multiple comparisons test (following ANOVA) was computed in GraphPad Prism (version 9.1.1). "ns" denotes "not significant".

$K_{d,eq} = C_{s,eq}/C_{w,eq}$	Atrazine	DEA	DIA	OH-ATZ	
$K_{d,eq}$ [L/g]	807.24 \pm 159.4	151.01 \pm 16.63	203.44 \pm 14.19	439.23 \pm 82.72	
	Imidacloprid	Desnitro-IMI	IMI-Urea	IMI-Olefin	Clothianidin
$K_{d,eq}$ [L/g]	1061.55 \pm 141.15	772.54 \pm 63.43	279.52 \pm 45.72	890.55 \pm 172.37	1112.03 \pm 250.86
Tukey's multiple comparisons test	Mean Diff.	95.00% CI of diff.	Below threshold?	Summary	Adjusted P Value
Atrazine vs. Imidacloprid	-254.3	-663.2 to 154.5	No	ns	0.4334
Atrazine vs. Clothianidin	-304.8	-713.6 to 104.1	No	ns	0.2345
Atrazine vs. DEA	656.2	283.0 to 1029	Yes	***	0.0004
Atrazine vs. DIA	603.8	230.6 to 977.0	Yes	***	0.0009
Atrazine vs. OH-ATZ	368.0	-5.221 to 741.2	No	ns	0.0547
Imidacloprid vs. Clothianidin	-50.48	-459.3 to 358.4	No	ns	>0.9999
Imidacloprid vs. Desnitro-IMI	289.0	-84.22 to 662.2	No	ns	0.1998
Imidacloprid vs. IMI-Urea	782.0	408.8 to 1155	Yes	****	<0.0001
Imidacloprid vs. IMI-Olefin	171.0	-202.2 to 544.2	No	ns	0.7682
DEA vs. DIA	-52.43	-386.3 to 281.4	No	ns	0.9996
DEA vs. OH-ATZ	-288.2	-622.0 to 45.61	No	ns	0.1185
DIA vs. OH-ATZ	-235.8	-569.6 to 98.04	No	ns	0.2888
Desnitro-IMI vs. IMI-Urea	493.0	159.2 to 826.8	Yes	**	0.0021
Desnitro-IMI vs. IMI-Olefin	-118.0	-451.8 to 215.8	No	ns	0.9259
IMI-Urea vs. IMI-Olefin	-611.0	-944.9 to -277.2	Yes	***	0.0002

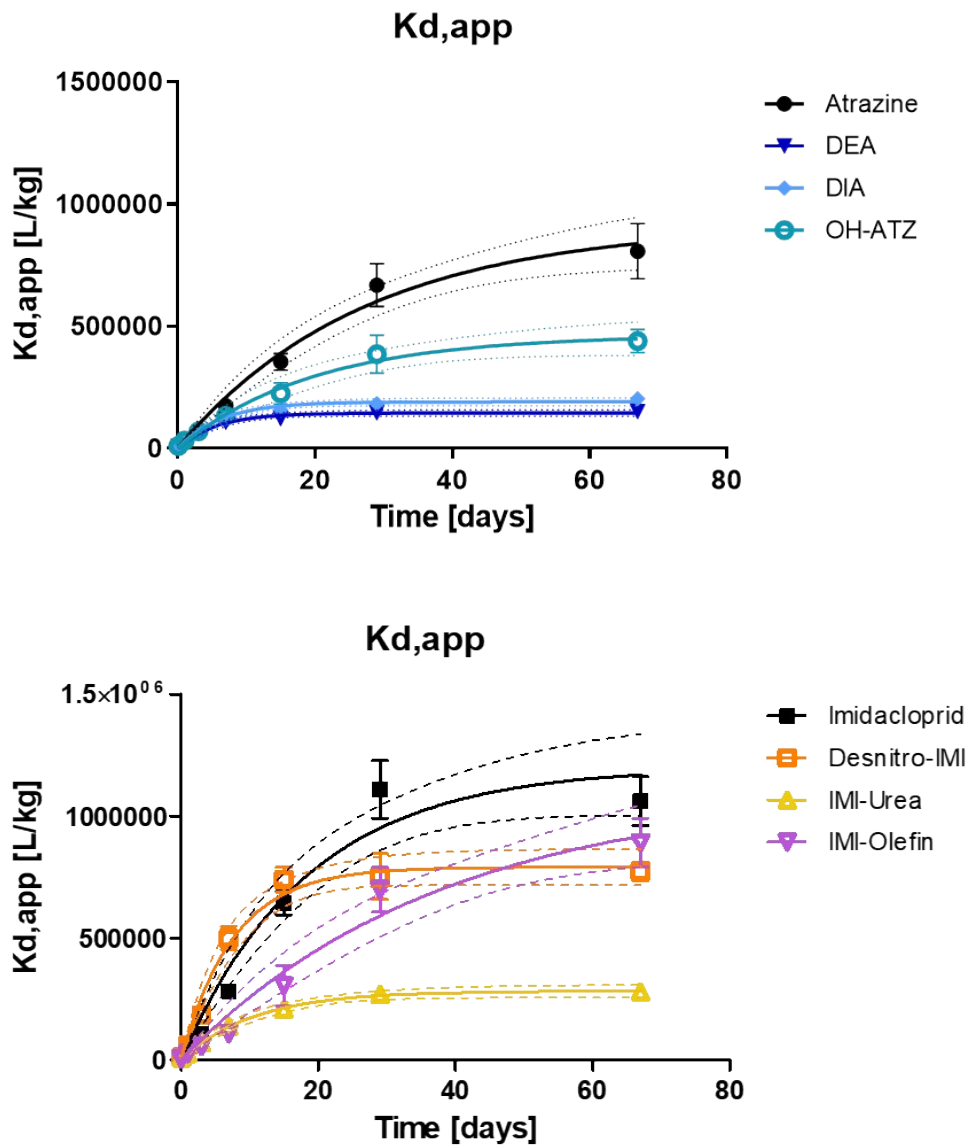


Figure S5: Kinetic batch sorption data plotted as apparent distribution coefficient, $K_d = C_s/C_w$ (C_s = sorbed concentration, C_w = aqueous concentration). The solid lines represent pseudo-first order fits and the dashed lines represent the 95% confidence intervals; the fit was simply done for better visualization.

5. Column Experiments

Salt Tracer Data

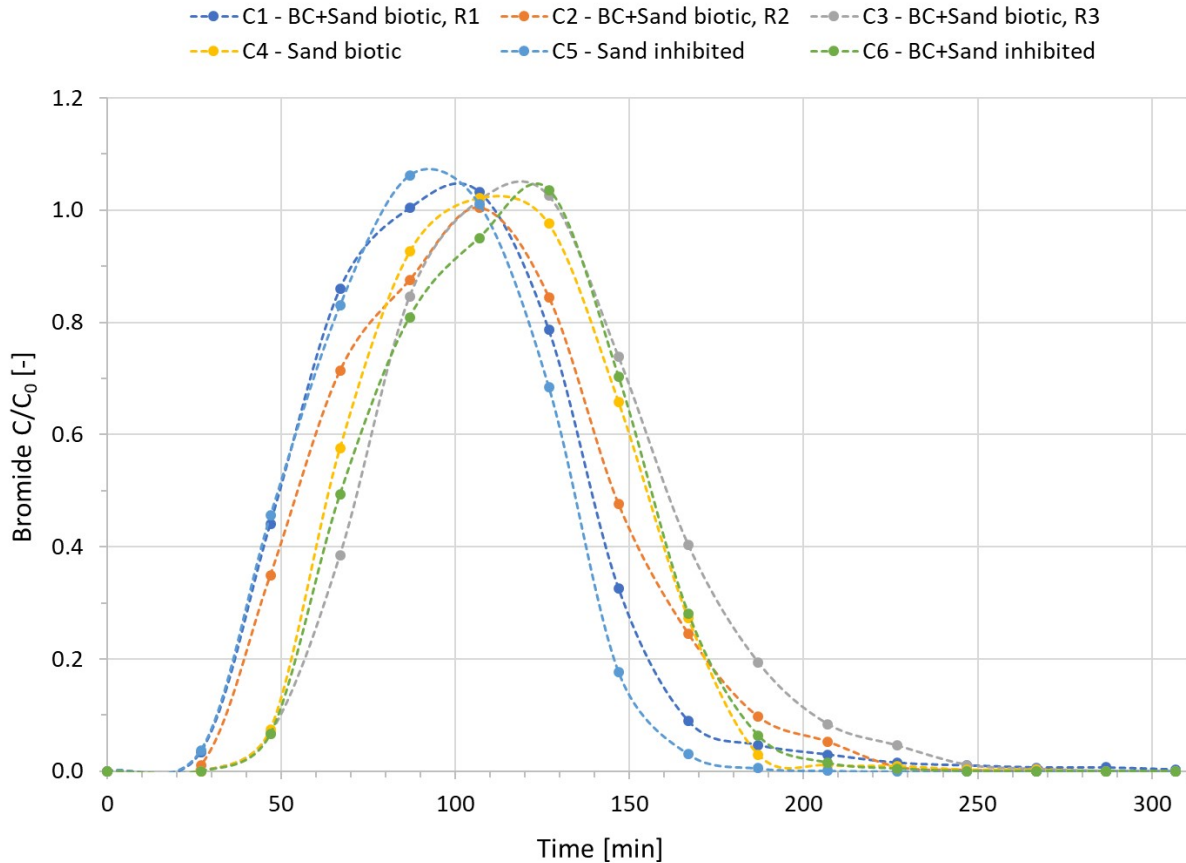


Figure S6: Salt tracer breakthrough curves in column effluents using a potassium bromide (KBr) tracer. Data is adjusted for hold-up time outside of porous media; ideal plug-flow conditions were assumed in tubing and in glass beads/glass wool mixture at the in- & outlet of columns.

Growth procedure of microbial enrichment solutions (multi-cycle inoculation)

Local sediment-creek water slurries served as the inoculum to the enrichment solutions. Duplicates of 1 L creek water each containing 100 mL of creek sediment, leaves, and silt were collected and let sit at room temperature overnight. Slurries were put on a shaker table for 24 h for pre-equilibration and were then centrifuged at 800 RCF for 5 min to remove large particles and leaves.

All supernatant was combined and transferred to a glass bottle for storage. Microbial cultures for the enrichment solutions were grown over two stages of three successive inoculation-incubation cycles as follows: Initial cultures were prepared by combining 100 mL of autoclaved DOC extract solution (~250 mg/L) with 10 mL of sediment-creek water inoculum in 500 mL Erlenmeyer flasks and aerobically incubated at 30°C on a shaker table in the dark. Growth of cultures was monitored visually (see Figure S7) and by measurement of the optical density (O.D.) every 2-3 days. After one week (7 d), cultures of the second cycle were prepared by combining 10 mL of the initial cultures with 100 mL of autoclaved DOC growth media and inoculated for another week (9 d). For the third cycle, the entire 110 mL of media was transferred to a 2000 mL Erlenmeyer flask containing 500 mL of autoclaved DOC extract solution and incubated again. The second incubation stage was carried out following the same method as described in the first stage, except for the following modifications: The DOC concentration of the growth media was higher (~650 mg/L), incubation cycles only lasted four days, and O.D. measurements were taken daily. O.D. values increased considerably 1-2 days after the culture was transferred to a new DOC growth media and dropped afterwards due to pronounced aggregation (see Figure S8). This observation reemphasizes the need to consider that O.D. measurements are only suitable for assessing growth of microbial cultures in the aqueous phase, as aggregates quickly sink to the bottom of the measurement cuvette and are hence not detected by the optical measurement.



Figure S7: Seeding cultures used for column inoculation and microcosms during the last stage (4 days) of the second inoculation cycle. Optical density (O.D.) at 600 nm of the culture was measured in a subsample each day and was as follows (chronological order): a) 0.183, b) 0.585, c) 0.643, d) 0.474. The seeding culture depicted in d) was used for column and microcosms inoculation the following day.

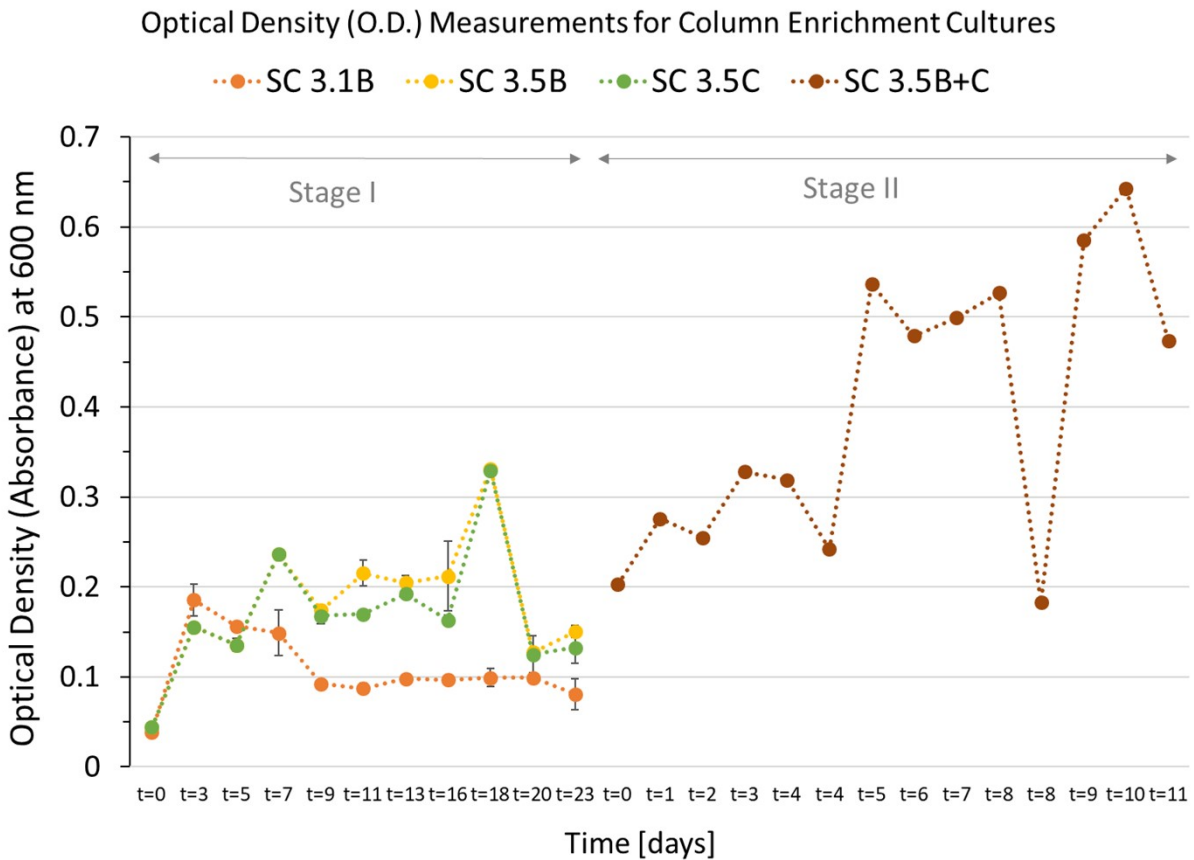


Figure S8: Optical density (O.D.) measurements of column enrichment cultures. In the beginning, several replicate batches were incubated and only the ones with most observed growth (highest O.D. values) were kept for continued multi-cycle inoculation. Cultures 3.5B and 3.5C were combined for stage II incubation, which resulted in the final culture 3.5B+C. Error bars during stage I represent standard deviation occurring from repeated measurement of the same sample (analytical variability).

6. Transformation Products & Suspect Screening

Suspect Compounds in Microcosms

Three suspect TPs were identified in microcosm (and column) samples: 5-hydroxy-imidacloprid (5-OH-IMI; Figure S9), nitrosoguanidine-imidacloprid (NG-IMI; Figure S10), and clothianidin-urea (CLO-urea; Figure S11).

The *absolute* average precursor mass error (in ppm) in Table S6 was calculated based on the suspect peaks identified in 20 microcosm samples total: for both biotic replicates (M1, M2), we analyzed five time points each (T8, T13, T15, T17, T19), while each sample was analyzed twice (R1, R2).

Table S6: MRM transitions of suspect analytes (all in ESI+ mode): The exact precursor mass was used for compound identification and at least one of the exact fragment masses was used for compound verification. The level of suspect confidence refers to the scale proposed by E. Schymanski (Schymanski et al. 2014).

Compound name	Formula	Precursor Mass (Q1) [Da] [M+H] ⁺	Av. Mass error [ppm]	Fragment Mass 1 (Q3) [Da]	Fragment Mass 2 (Q3) [Da]	RT [min]	Fragments [Da], Literature	Confidence level (Schymanski)
5-Hydroxy-Imidacloprid (5-OH-IMI)	C ₉ H ₁₀ ClN ₅ O ₃	272.05449	1.41	225.0569	191.0949	5.13	225, 191 [†]	Level 4
Nitrosoguanidine-Imidacloprid (NG-IMI) or Nitrosoimine-Imidacloprid	C ₉ H ₁₀ ClN ₅ O	240.06466	1.42	209.0591	175.0981	5.09	209, 175, 84 [‡]	Level 3
Clothianidin-Urea (CLO-urea or TZMU)	C ₆ H ₈ ClN ₃ OS	206.01494	0.80	131.9671	119.9675	4.67	131.97, 120.01 [§]	Level 3
References:								
† Giroud et al. 2013; ‡ Schulz-Jander et al. 2002; Dick et al. 2006; § Sánchez-Hernández et al. 2016; Kim et al. 2012								

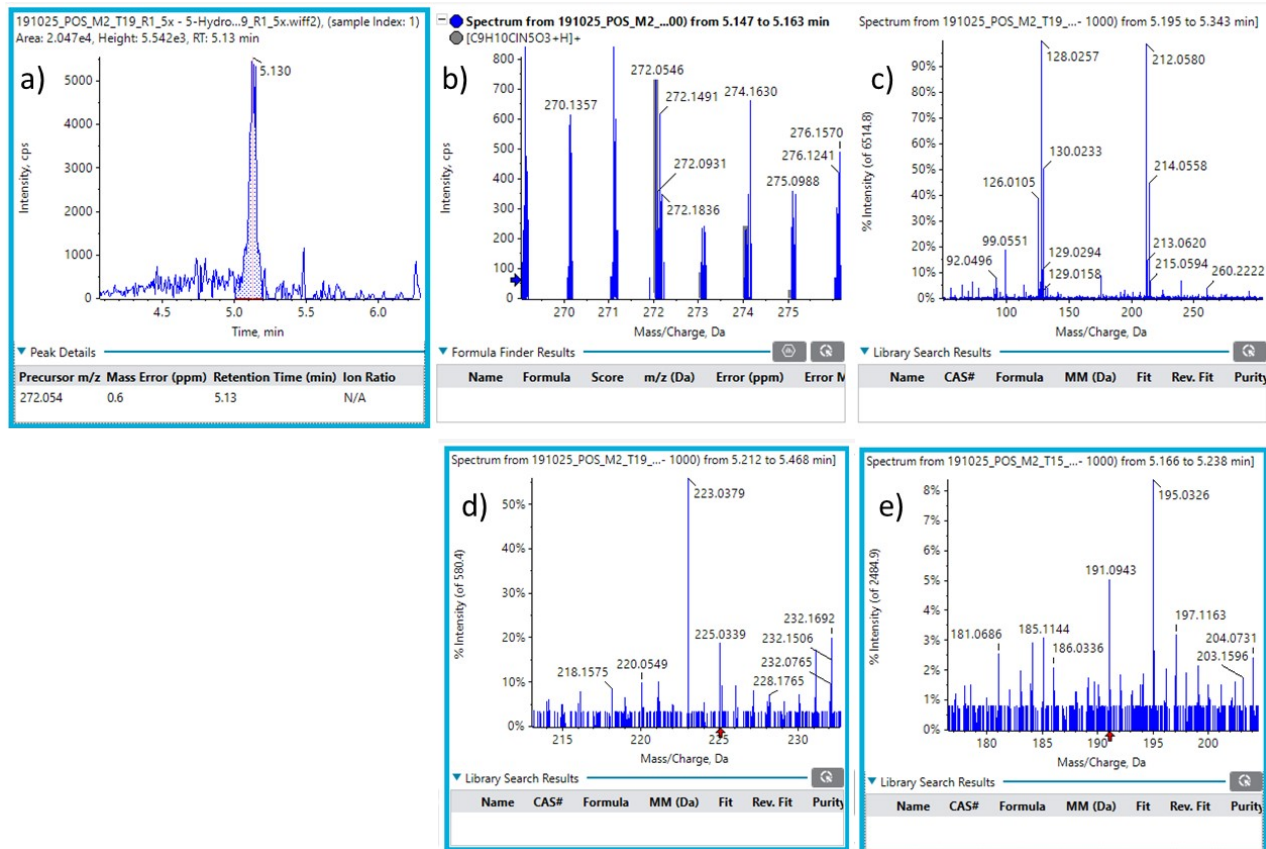


Figure S9: Representative MS and MS² scans for 5-Hydroxyimidacloprid. a) Precursor ion extracted chromatogram, b) Isotope spectrum of precursor ion, c) MS² scan, d) Zoomed in MS² scan at 225.05 Da (fragment), e) Zoomed in MS² scan at 191.09 Da (fragment).

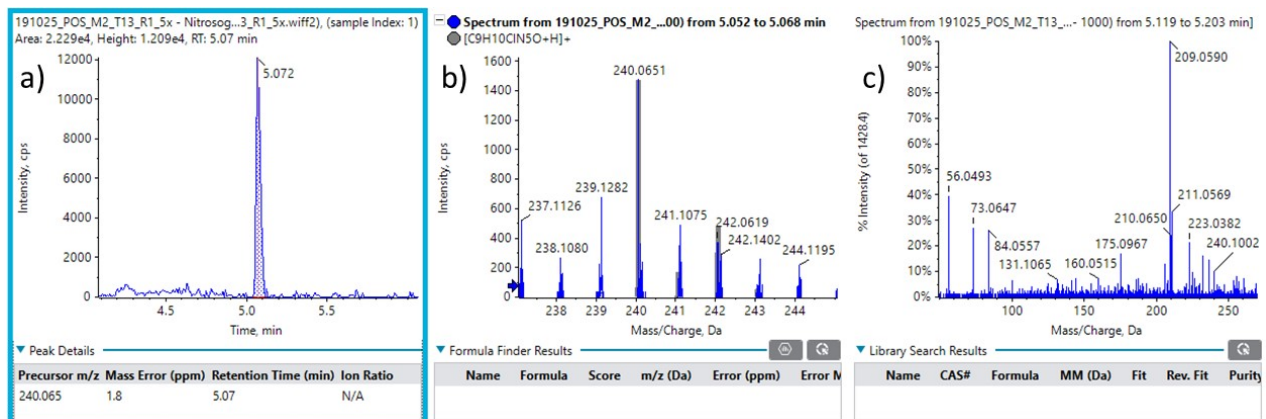


Figure S10: Representative MS and MS² scans for Nitrosoguanidine-Imidacloprid. a) Precursor ion extracted chromatogram, b) Isotope spectrum of precursor ion, c) MS² scan including fragments at 209.05 Da and 175.09 Da.

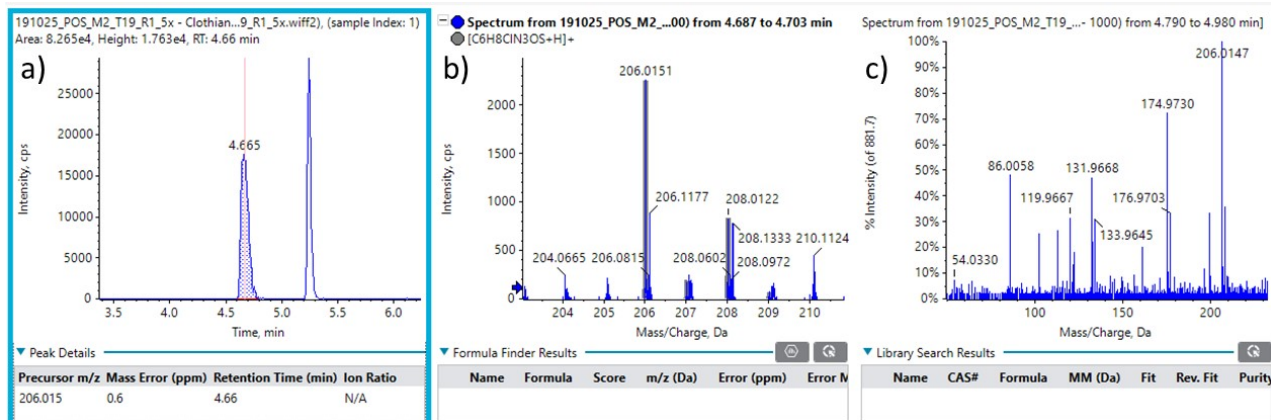


Figure S11: Representative MS and MS² scans for Clothianidin-Urea. a) Precursor ion extracted chromatogram, b) Isotope spectrum of precursor ion, c) MS² scan including fragments at 131.96 Da and 119.96 Da.

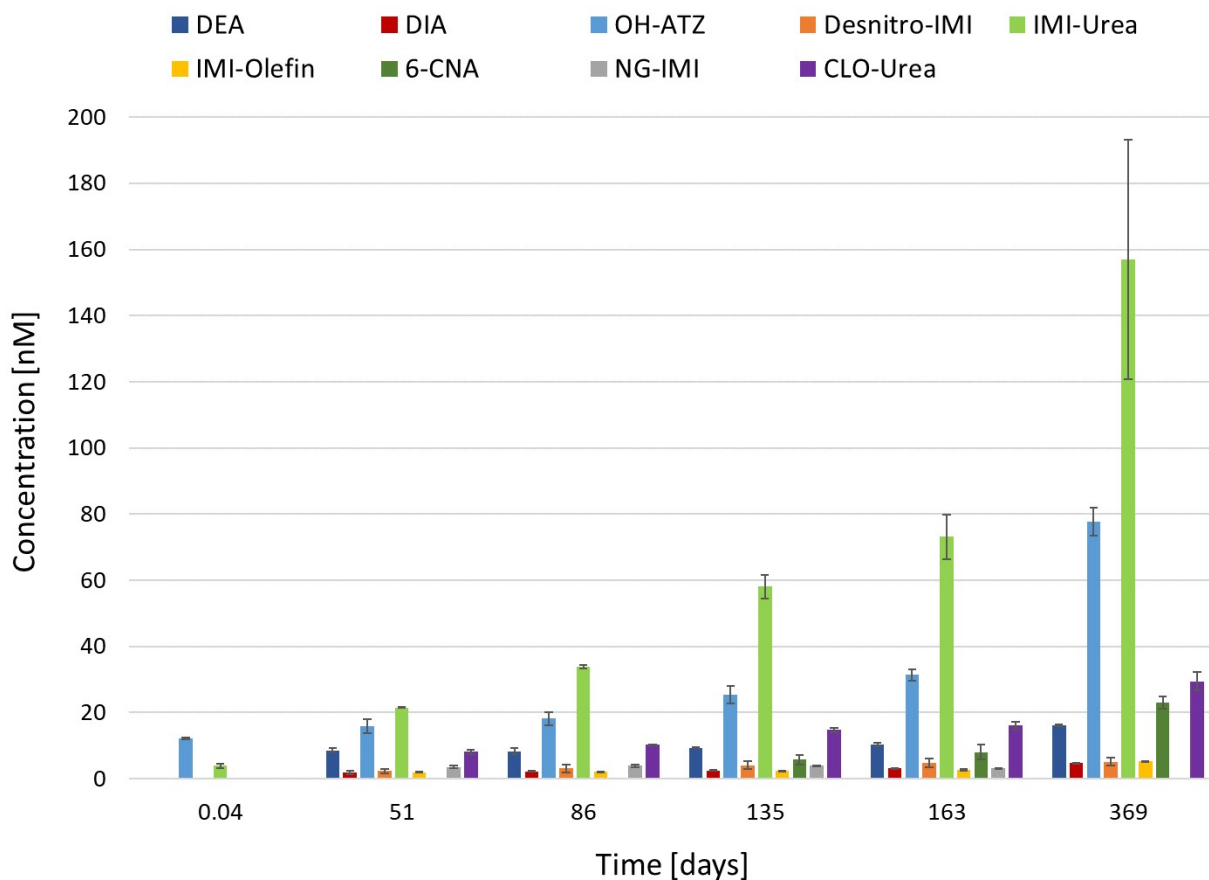


Figure S12: Target and suspect transformation products in microcosms over time. Error bars represent the standard deviation between experimental replicates (n=2). Abbreviations: desethylatrazine (DEA), desisopropylatrazine (DIA), and 2-hydroxyatrazine (OH-ATZ), desnitro-imidacloprid (desnitro-IMI), imidacloprid-urea (IMI-urea), imidacloprid-olefin (IMI-olefin), 6-chloronicotinic acid (6-CNA), nitrosoguanidine-imidacloprid (NG-IMI), and clothianidin-urea (CLO-urea). Note that concentrations for NG-IMI and CLO-urea are semi-quantitative.

Additional Transformation Products & Suspect Compounds in Columns

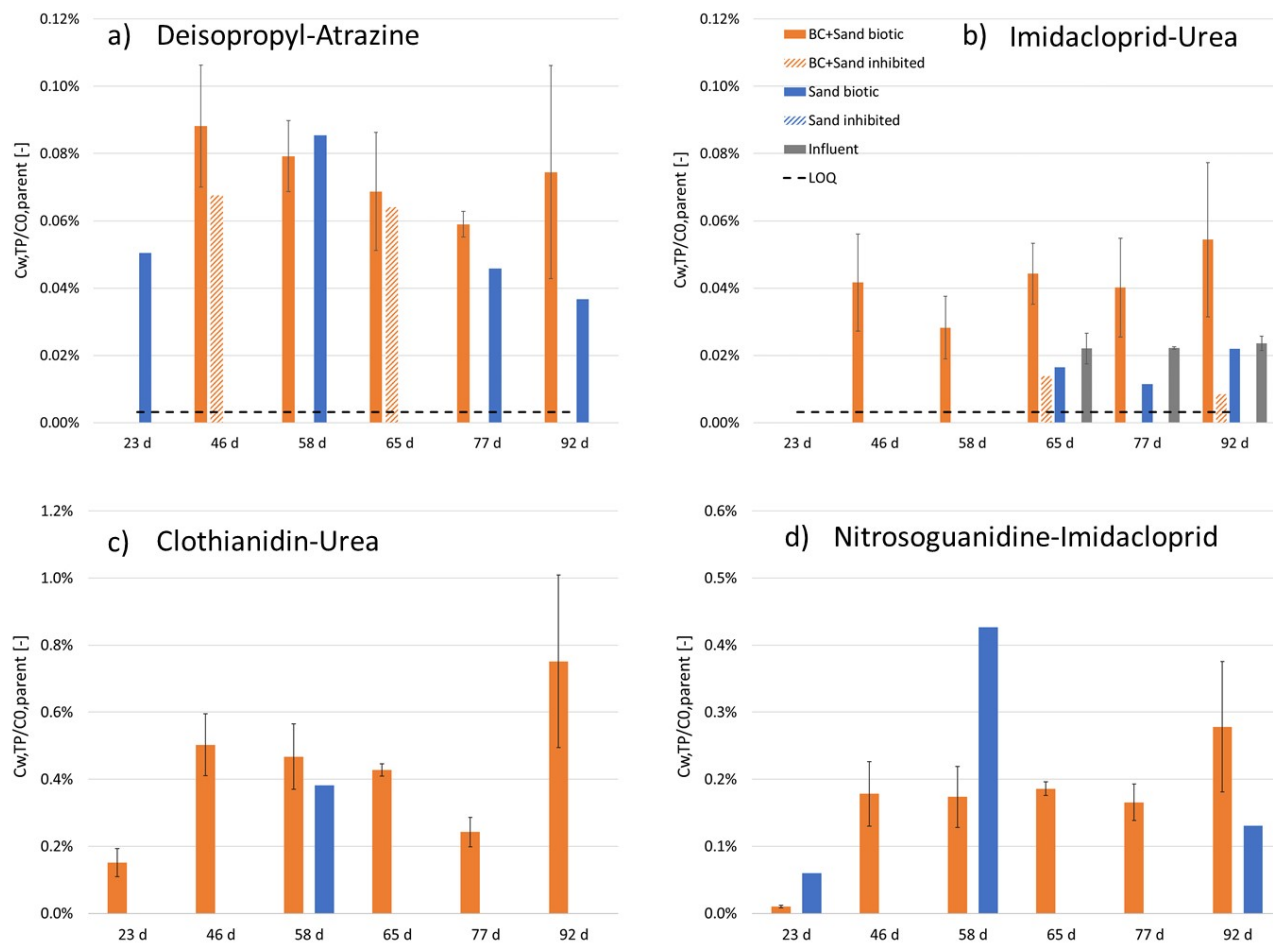


Figure S13: Additional target and suspect transformation products (TPs) of atrazine, imidacloprid, and clothianidin in column effluents (and influent) identified by LC-QToF-MS analysis: a) deisopropyl-atrazine, b) imidacloprid-urea, c) clothianidin-urea (suspect; semi-quantitative), d) nitrosoguanidine-imidacloprid (suspect; semi-quantitative). Y-axis shows TP concentrations normalized by the average parent influent concentration ($C_{w,TP}/C_{0,parent}$). Dotted black lines represent the limit of quantitation (LOQ) for each TP (not available for suspects).

Semi-Quantitation

Approach:

1) Choose calibrant matches for all suspect compounds. Ideally, the calibrant has similar or the same ionizable groups as the suspect. We chose imidacloprid as the calibrant for 5-OH-IMI and NG-IMI, and clothianidin was the calibrant for CLO-urea.

2) Determine a response factor (RF) for each calibrant (= slope of calibration curve). When using internal standards (IS), this is actually a relative response factor to the IS.

$$C_{suspect} = \frac{Area_{suspect} * C_{IS}}{Area_{IS} * RF} * \frac{MW_{suspect}}{MW_{calibrant}}$$

3) Calculate the suspect concentration:

where $C_{IS} = 1$ (relative concentration of IS in samples vs. in standards) and MW refers to the molecular weight of compounds.

Further, it is essential that both calibrant and suspect compounds were acquired with the same extracted ion chromatogram (XIC) window; in our study 0.02 Da was used consistently.

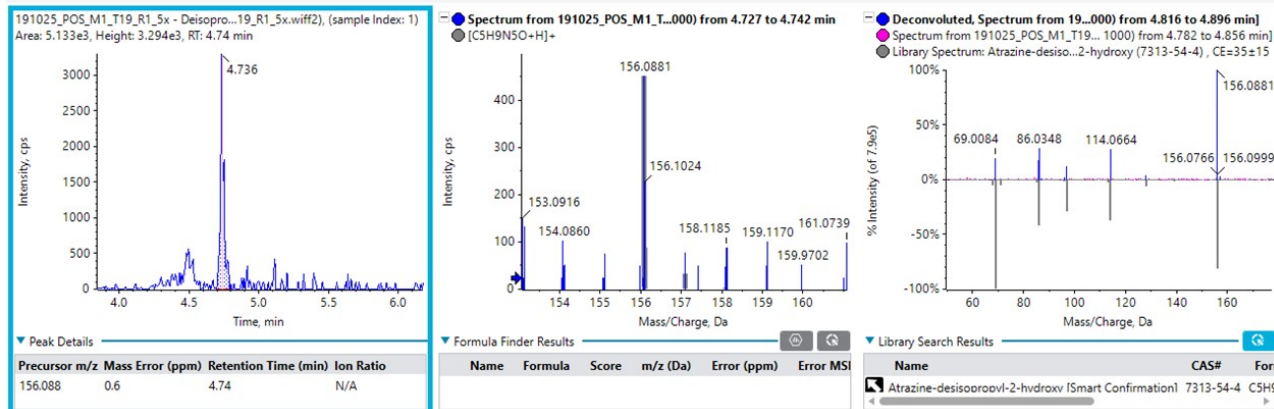
Target and Suspect Transformation Products in Columns and Microcosms

Table S7: Range of (average) concentrations observed in the biotic BC+Sand columns and in the microcosms. Please note that concentrations for NG-IMI and CLO-urea are semi-quantitative.

Transformation product	Columns (BC+Sand biotic) [µg/L]	Microcosms [µg/L]
Desethyl-atrazine (DEA)	<i>n.d.</i> - 0.147	<i>n.d.</i> - 3.015
Deisopropyl-atrazine (DIA)	<i>n.d.</i> - 0.138	<i>n.d.</i> - 0.817
2-Hydroxy-atrazine (OH-ATZ)	0.037 - 3.192	2.41 - 15.343
Desnitro-imidacloprid (Desnitro-IMI)	<i>n.d.</i> - 0.448	<i>n.d.</i> - 1.075
Imidacloprid-urea (IMI-urea)	<i>n.d.</i> - 0.084	0.833 - 33.206
Imidacloprid-olefin (IMI-olefin)	<i>n.d.</i> - 0.298	<i>n.d.</i> - 1.348
6-chloronicotinic acid (6-CNA)	<i>n.d.</i> - 0.091	<i>n.d.</i> - 3.616
Nitrosoguanidine-imidacloprid (NG-IMI)	0.018 - 0.487	<i>n.d.</i> - 0.946
Clothianidin-urea (CLO-urea)	0.236 - 1.171	<i>n.d.</i> - 6.053

In-Source Fragmentation

a) Sample (RT=4.73 min):



b) Analytical standard (RT=4.73 min):

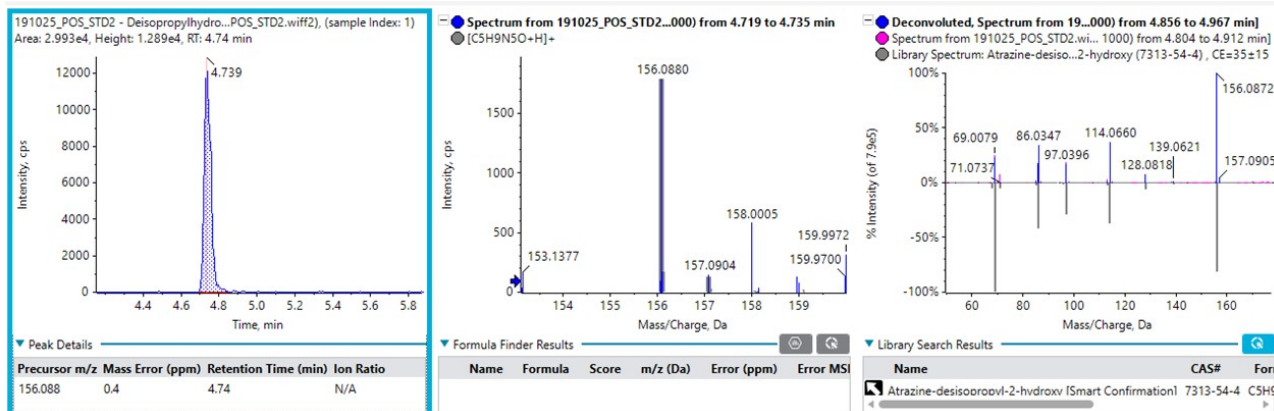
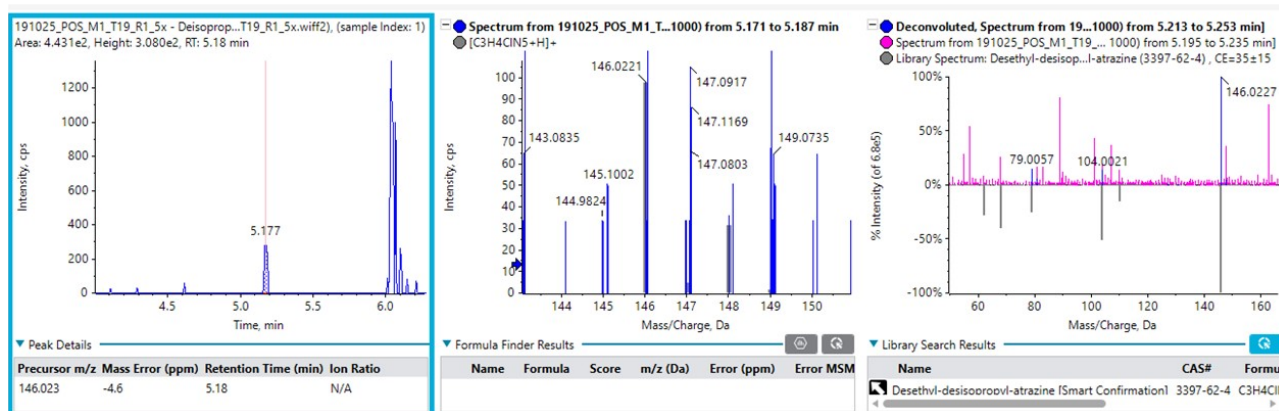


Figure S14: The suspect deisopropylhydroxy-atrazine as a product of in-source fragmentation of 2-hydroxy-atrazine (OH-ATZ) at identical retention times of 4.73 min, found both in microcosm samples (a) and analytical standards (b). Both precursor peaks were confirmed by library hits (score >99).

a) Sample (RT=5.17 min):



b) Analytical standard (RT=5.17 min and 4.67 min):

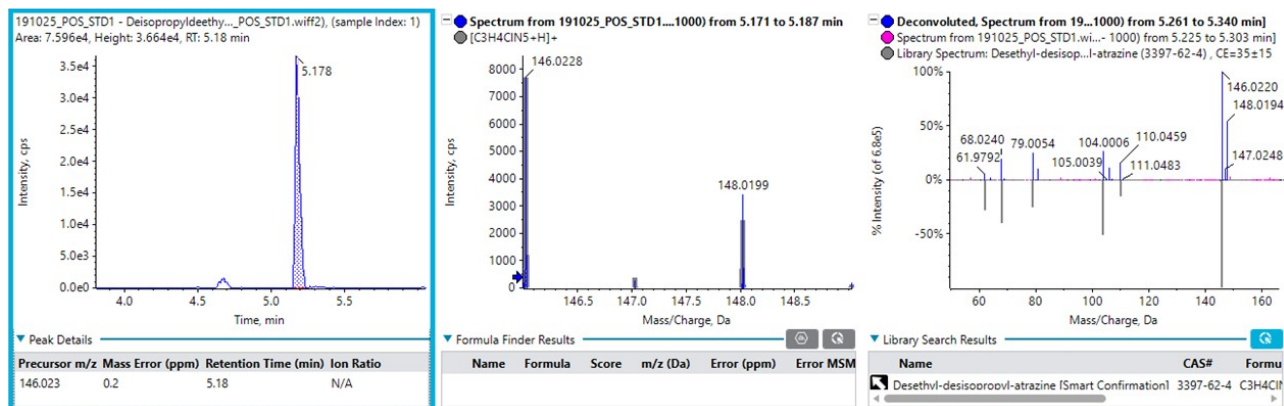


Figure S15: The suspect desethyldeisopropyl-atrazine (or didealkyl-atrazine) as a product of in-source fragmentation of desethyl-atrazine (DEA) at identical retention times of 5.17 min, found both in microcosm samples (a) and analytical standards (b). Both precursor peaks were confirmed by library hits (score >93). The peak to the left in panel b) is the product of in-source fragmentation of deisopropyl-atrazine (DIA) in the analytical standard, but was not found in the sample.

7. Transport Modelling

Column Pollutant Transport Model

The column model considers pollutant transport by advection and dispersion of mobile water in addition to the sorption and biodegradation processes. Two types of column medium particles are considered, non-porous S particles (i.e. sand) and porous BC particles (i.e. biochar or activated carbon). The instantaneous equilibrium model assumes local sorption equilibrium between mobile water and these particles, whereas the kinetic sorption model considers first-order rate uptake of pollutants by the S particles, and pollutant diffusion in the water-filled pore network of the BC particles retarded by sorption to the BC solid matrix. Biodegradation of pollutants is assumed to occur in the water in between the S and BC particles and is described by first-order rate biodegradation kinetics. Parameters are expressed in SI units of moles, seconds, kilograms, and meters (Table S8). The pollutant concentration in the mobile water in between the S and BC particles, C_w , the pollutant concentration in the S particles, C_s , and the pollutant concentration in the BC intraparticle porewater $C_{BC,ippw}$, are all dependent on the distance from the column inlet x , and time t . $C_{BC,ippw}$ additionally varies as a function of the distance r from the particle centre.

Table S8: Independent and dependent column model variables and input parameters and their dimensions.

t (s)	Time
x (m)	Distance from the column inlet
r (m)	Radial distance from the BC particle centre
L (m)	Length of the column
R (m)	Radius of the column
θ_s (-)	Volume fraction of the column filled with S particles
θ_{BC} (-)	Volume fraction of the column filled with BC particles
θ_w (-)	Volume fraction of the column filled with mobile water (water in between the S and BC particles)
C_w (moles m^{-3})	Pollutant concentration in the mobile water in the column (water in between the BC and S particles)

C_{in} (moles m^{-3})	Pollutant concentration in the column influent
C_S (moles kg^{-1})	Pollutant concentration associated with the S particles
$C_{BC,solid}$ (moles kg^{-1})	Pollutant concentration in the BC solid matrix
$C_{BC,ippw}$ (moles m^{-3})	Pollutant concentration in the BC intraparticle porewater
$C_{min,Fr}$ (moles m^{-3})	Pollutant concentration in the BC intraparticle porewater below which an alternative isotherm model is substituted to avoid division by zero.
K_S (m^3kg^{-1})	S particle-water partitioning coefficient for the pollutant
k_S (s^{-1})	First-order kinetic sorption rate for pollutants sorbed by the S particles
$K_{Fr,BC}$ (moles kg^{-1} (m^3 moles $^{-1}$) $1/n_{Fr,BC}$)	Freundlich isotherm coefficient for the pollutant
$n = 1/n_{Fr,BC}$ (-)	Freundlich isotherm exponent for the pollutant
k_{deg} (s^{-1})	First-order biodegradation rate for the pollutant in the mobile water (in between the S and BC particles)
v_x (ms^{-1})	Velocity of the mobile water flowing in between the S and BC particles in the x direction
D_{disp} (m^2s^{-1})	Dispersion coefficient for pollutants in the mobile water flowing in between the S and BC particles in the x direction
M_S (kg)	Dry mass of S particles in the column
d_S ($kg m^{-3}$)	Solid density of the S particles
M_{BC} (kg)	Dry BC mass in the column
R_{BC} (m)	BC particle radius
$\theta_{BC,ippw}$ (-)	Water-filled BC intraparticle porosity
d_{BC} ($kg m^{-3}$)	Solid density of the BC skeleton/solid matrix
τ_{BC} (-)	BC pore network tortuosity factor
D_{aq} (m^2s^{-1})	The molecular diffusion coefficient of the pollutant in water

Column medium composition:

The volume fraction of the column filled with S particles, θ_s , can be calculated as

$$\theta_s = \frac{M_s}{d_s L \pi R^2} \quad \text{eq 1}$$

where M_S is the dry mass of S particles in the column, d_S is the S particle density, L is the column length and R the column radius.

The volume fraction of the column filled with BC particles, θ_{BC} , can be calculated as

$$\theta_{BC} = \frac{M_{BC}}{(1 - \theta_{BC,ippw})d_{BC}L\pi R^2} \quad \text{eq 2}$$

where M_{BC} is the dry mass of BC particles in the column, $\theta_{BC,ippw}$ is the water-filled intraparticle porosity, and d_{BC} is the density of the solid matrix of the BC particles.

The volume fraction of the column space in between the S and BC particles, which is assumed to be filled with mobile water, θ_w , can be calculated as

$$\theta_w = 1 - \theta_s - \theta_{BC} \quad \text{eq 3}$$

Intraparticle diffusion of the pollutant in the pore network of BC particles:

Freundlich isotherm model:

The Freundlich isotherm model describes the sorption equilibrium distribution of pollutants between water and the BC solid matrix

$$C_{BC,solid} = K_{Fr} \cdot (C_{BC,ippw})^{1/n_{Fr,BC}} \quad \text{eq 4}$$

where $C_{BC,solid}$ is the pollutant concentration in the solid matrix of the BC particles, $C_{BC,ippw}$ is the pollutant concentration in the intraparticle porewater of the BC particles, $K_{Fr,BC}$ is the Freundlich isotherm coefficient for the pollutant sorption by the BC solid matrix, and $1/n_{Fr,BC}$ is the Freundlich exponent. To avoid issues with the derivative when $C_{BC,ippw}$ is zero, the Freundlich isotherm is substituted with an alternative isotherm below a threshold intraparticle concentration value $C_{min,Fr}$

$$C_{BC,solid} = a \cdot C_{BC,ippw} + b \cdot (C_{BC,ippw})^2 \quad \text{eq 5}$$

Parameters a and b are chosen so that the substituted isotherm has the same value and slope as the Freundlich isotherm at $C_{BC,ippw} = C_{min,Fr}$.

Effective diffusion coefficient:

The effective diffusion coefficient of the pollutant in the BC particle pore network is defined as

$$D_{eff,BC} = \frac{\theta_{BC,ippw} \cdot D_{aq}}{\tau_{BC}} \quad \text{eq 6}$$

where τ_{BC} is the BC particle pore network tortuosity factor, $\theta_{BC,ippw}$ the intraparticle porosity of the BC particles, which is assumed to be filled with immobile water, and D_{aq} is the molecular diffusion coefficient of the pollutant in water.

The following partial differential equation governs the pollutant concentration in BC intraparticle pore water, $C_{BC,ippw}$, for the Freundlich isotherm model

$$\begin{aligned} \frac{d}{dt} \left(\theta_{BC,ippw} \cdot C_{BC,ippw} + (1 - \theta_{BC,ippw}) \cdot d_{BC} \cdot K_{Fr,BC} \cdot (C_{BC,ippw})^{1/n_{Fr,BC}} \right) \\ = \frac{D_{eff,BC}}{r^2} \cdot \frac{\partial}{\partial r} r^2 \frac{\partial}{\partial r} C_{BC,ippw} \end{aligned} \quad \text{eq 7}$$

Differentiation of the left-hand side results in

$$\begin{aligned} \left(\theta_{BC,ippw} + (1 - \theta_{BC,ippw}) \cdot d_{BC} \cdot K_{Fr,BC} \cdot (C_{BC,ippw})^{(1/n_{Fr,BC} - 1)} \cdot \frac{1}{n_{Fr,BC}} \right) \cdot \frac{d}{dt} C_{BC,ippw} \\ = \frac{D_{eff,BC}}{r^2} \cdot \frac{\partial}{\partial r} r^2 \frac{\partial}{\partial r} C_{BC,ippw} \end{aligned}$$

eq 8

Pollutant mass transfer from BC particles to the mobile water in the column (in between the S and BC particles):

The BC particles to mobile water pollutant mass transfer rate, $\Gamma_{ippwd,out}$, is described by

$$r_{ippwd,out} = -\frac{\theta_{BC}}{\frac{4}{3}\pi R_{BC}^3} \cdot 4\pi R_{BC}^2 \cdot D_{eff,BC} \cdot \frac{\partial}{\partial r} C_{BC,ippw} \Big|_{r=R_{BC}} = -3 \frac{\theta_{BC}}{R_{BC}} \cdot D_{eff,BC} \cdot \frac{\partial}{\partial r} C_{BC,ippw} \Big|_{r=R_{BC}}$$

eq 9

Where R_{BC} is the BC particle radius.

Pollutant mass transfer from the mobile water in the column (in between the S and BC particles)

to the S particles:

The following differential equation governs the pollutant concentration in S particles

$$\theta_S d_S \cdot \frac{d}{dt} C_S = r_S = -\theta_w k_S \left(\frac{C_S}{K_S} - C_w \right) \quad \text{eq 10}$$

where k_S is the first-order kinetic sorption rate, and K_S the linear S particle to water partitioning coefficient for the pollutant.

Pollutant removal by biodegradation from the mobile water in the column (in between the S and

BC particles):

The first-order pollutant mass removal rate from mobile water by biodegradation, r_{deg} , is described by

$$r_{deg} = \theta_w k_{deg} C_w \quad \text{eq 11}$$

where k_{deg} is a first-order biodegradation rate for the pollutant in mobile water.

Pollutant fate in mobile water in the column (in between the S and BC particles) for the kinetic sorption model:

The following partial differential equation governs the pollutant concentration in the mobile water phase for the kinetic sorption model:

$$\theta_w \cdot \frac{d}{dt} C_w = \theta_w D_{disp} \frac{\partial^2}{\partial x^2} C_w - \theta_w v_x \frac{\partial}{\partial x} C_w + r_{ippwd,out} - r_S - r_{deg} \quad \text{eq 12}$$

where D_{disp} is the dispersion coefficient for pollutants in the mobile water, and v_x is the velocity of this water when flowing within the column in between the S and BC particles in the x direction.

Pollutant fate in mobile water in the column (in between the S and BC particles) for the sorption equilibrium model:

The following partial differential equation governs the pollutant concentration in the mobile water phase for the instantaneous sorption equilibrium model:

$$\left(\theta_w + \theta_S \cdot d_S \cdot K_S + \theta_{BC} \cdot \theta_{BC,ippw} + \theta_{BC} \cdot (1 - \theta_{BC,ippw}) \cdot d_{BC} \cdot K_{Fr,BC} \cdot (C_w)^{\left(1/n_{Fr,BC} - 1\right)} \right) \cdot \frac{d}{dt} C_w = \theta_w D_{disp} \frac{\partial^2}{\partial x^2} C_w - \theta_w v_x \frac{\partial}{\partial x} C_w - r_{deg}$$

eq 13

Boundary conditions:

Column boundary conditions:

It was assumed that flux into the column is by advection only with influent concentration, C_{in} ,

$$\left(-D_{disp} \cdot \frac{\partial}{\partial x} C_w + v_x \cdot C_w \right) \Big|_{x=0} = v_x \cdot C_{in} \quad \text{eq 14}$$

and flux out of the column is also by advection only,

$$\left(-D_{disp} \cdot \frac{\partial}{\partial x} C_w + v_x \cdot C_w \right) \Big|_{x=L} = v_x \cdot C_w \quad \text{eq 15}$$

For the intraparticle diffusion model, a zero-concentration gradient boundary condition is enforced at $r=0$ in the centre of the BC particles due to the assumed spherical symmetry of the particles

$$\frac{\partial}{\partial r} C_{BC,ippw} \Big|_{r=0} = 0 \quad \text{eq 16}$$

and the pollutant concentration in BC intraparticle pore water at the mobile water-BC interface is set equal to the pollutant concentration in the mobile water phase, C_w , at the corresponding location within the column (i.e. it is assumed that there is no external aqueous film mass transfer resistance)

$$C_{BC,ippw}|_{r=R_{BC}} = C_w \quad \text{eq 17}$$

Input Parameters Column Model

Table S9: General input parameters for column transport model.

Parameter	Value	Common Units	Value	Model units (SI)	Comments
For all three pesticides					
Flow rate, Q	0.2114	[mL/min]	3.523E-09	[m3/s]	
Column length, L_c	5.6	[cm]	0.056	[m]	
Inner column radius, R_c	1.25	[cm]	0.0125	[m]	
Total dry mass of biochar in the column, M_bc	0.23665	[g]	0.00023665	[kg]	0.5wt% BC
Total dry mass of S particles in the column, M_s	47.33	[g]	0.04733	[kg]	Average value as measured during column packing
Skeletal density of biochar	1.7	[g/cm3]	1700	[kg/m3]	Ulrich et al., 2015
Sand solid density	2.54	[g/cm3]	2540	[kg/m3]	Ulrich et al., 2015
Biochar particle size	53-250	[µm]	(53-250)*10 ⁻⁶	[m]	Sieve sizes
Radius of biochar particle	57.6	[µm]	0.0000576	[m]	Geometric mean of particle size range
Sand particles size	210-297	[µm]	(210-297)*10 ⁻⁶	[m]	Per manufacturer
Radius of sand particle	126.75	[µm]	0.000127	[m]	Average value
Atrazine					
Molecular weight, MW	215.68	[g/mol]	215.68*10 ⁻³	[kg/mol]	
Influent concentration, cin	194.53	[µg/L]	0.000902	[moles/m3]	Average value over 92 days

Imidacloprid					
Molecular weight, MW	255.66	[g/mol]	$255.66 \cdot 10^{-3}$	[kg/mol]	
Influent concentration, C_{in}	187.10	[$\mu\text{g/L}$]	0.000732	[moles/m ³]	Average value over 92 days
Clothianidin					
Molecular weight, MW	249.68	[g/mol]	$249.68 \cdot 10^{-3}$	[kg/mol]	
Influent concentration, C_{in}	189.15	[$\mu\text{g/L}$]		[moles/m ³]	Average value over 92 days

Sorption to Sand Media

The sand partitioning coefficient (K_S) and the first-order kinetic sorption rate (k_S) for pollutants sorbed by the sand particles were estimated via best-fit to the inhibited Sand column data:

K_S [m³kg⁻¹] = 0.0028, 0.0011, and 0.0023 for atrazine, imidacloprid, and clothianidin.

k_S [s⁻¹] = 0.0025, 0.0253, and 0.0052 for atrazine, imidacloprid, and clothianidin.

Column Breakthrough Curve Predictions based on Batch Data

See Table S10 for the batch-derived input parameters (K_f , n , τ).

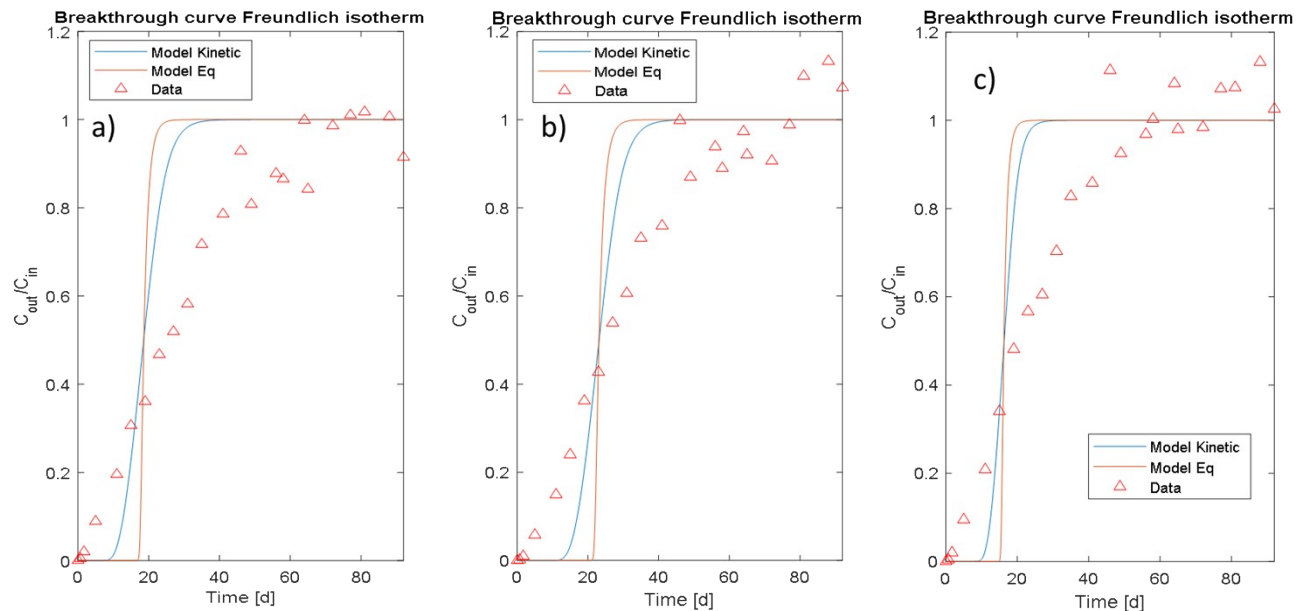


Figure S16: Prediction of *inhibited* BC+Sand column breakthrough curves using the batch-derived Freundlich sorption isotherm (K_f , n) and kinetic (tortuosity) parameters in the MATLAB transport model. a) Atrazine, b) imidacloprid, c) clothianidin.

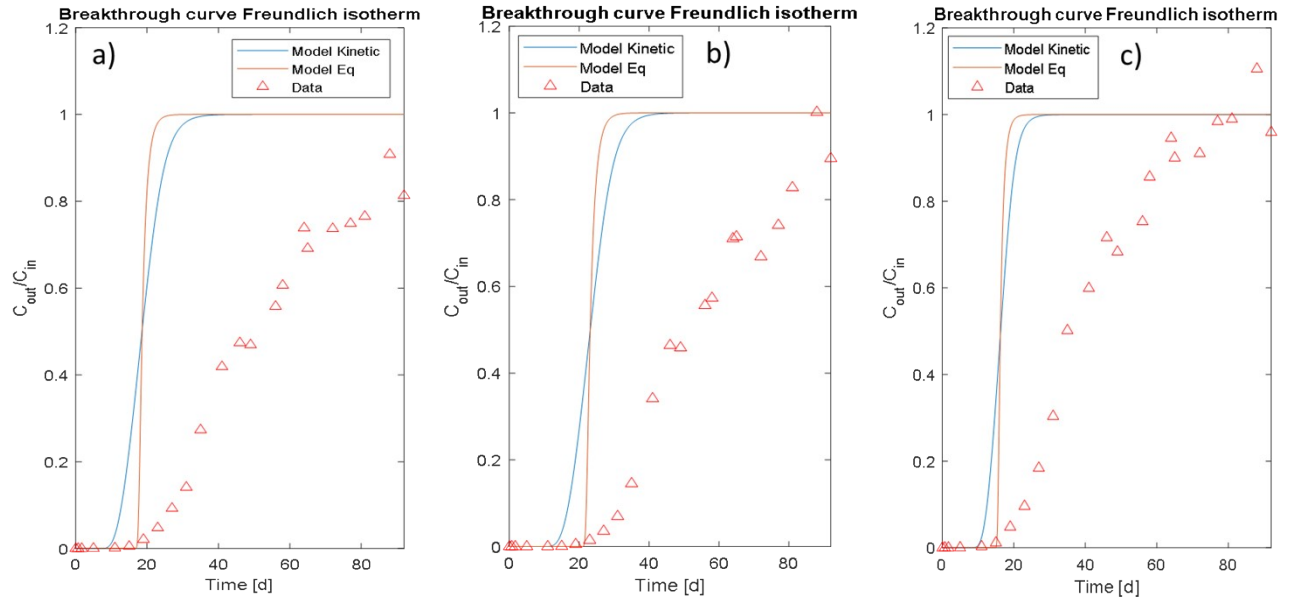


Figure S17: Prediction of *biotic* BC+Sand column breakthrough curves using the batch-derived Freundlich sorption isotherm (K_f , n) and kinetic (tortuosity) parameters in the MATLAB transport model. a) Atrazine, b) imidacloprid, c) clothianidin.

Parameter Estimation based on Column Data (Best-Fit)

See Table S10 for the best-fit parameters (K_f , n , τ) of the inhibited and biotic column data.

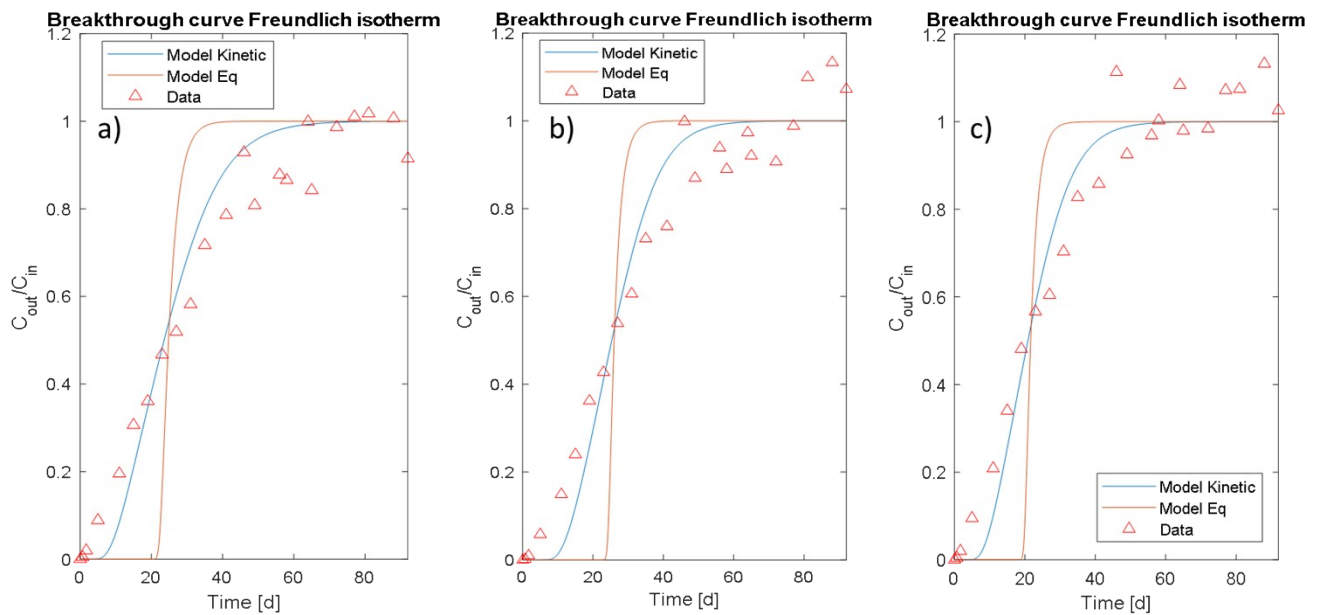


Figure S18: Best-fit simulations of *inhibited* BC+Sand column breakthrough curves using the transport model in MATLAB and assuming Freundlich non-linear sorption behavior. a) Atrazine, b) imidacloprid, c) clothianidin.

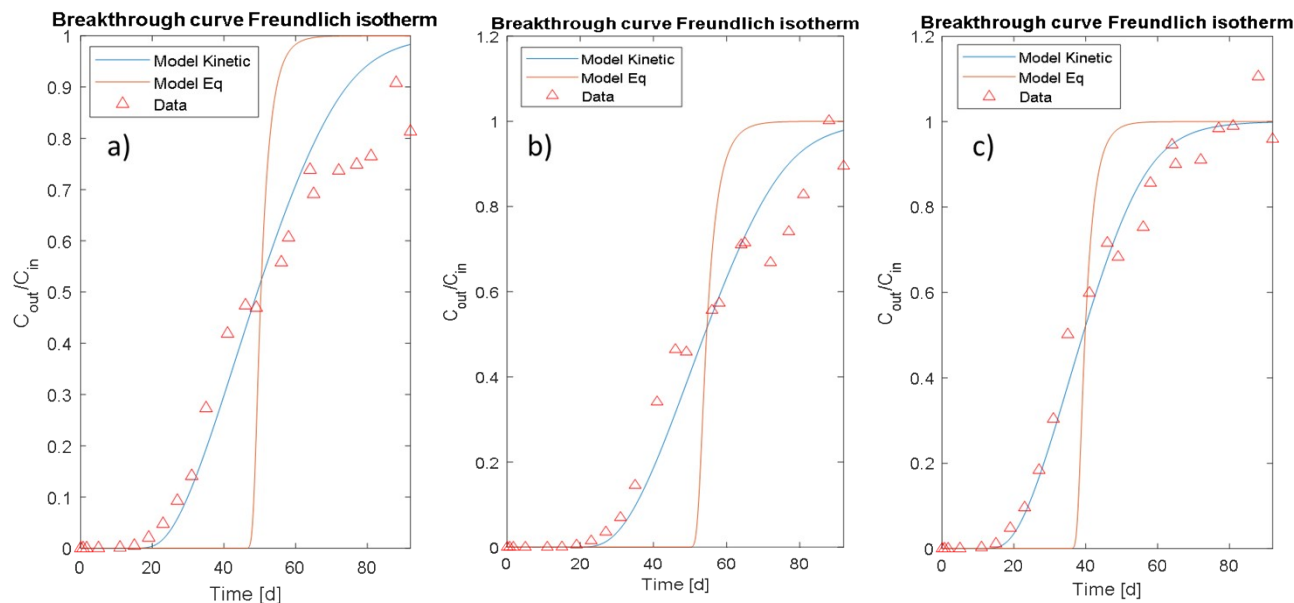


Figure S19: Best-fit simulations of biotic BC+Sand column breakthrough curves using the transport model in MATLAB and assuming Freundlich non-linear sorption behavior. a) Atrazine, b) imidacloprid, c) clothianidin.

Table S10: Freundlich sorption parameters, kinetic fitting parameter (tortuosity), goodness of fit, and linearized distribution coefficients for batch (abiotic) and column systems (inhibited and biotic) (Figures S16-S19).

Pesticide	Common units		Transport model units (SI units)		Kinetics	Goodness of fit	Linearization of isotherms (for comparison only)	
	Kf [(ug/g)/((ug/L)^n)]	n [-]	Kfr_bc [(moles/kg)*((m ³ /moles)^(1/nfr_bc))]	nfr_bc [-] (n = 1/nfr_bc)	Tortuosity, τ [-]	Sum of squared residuals, SSR [moles/kg]	K _d [L/kg] at C _w = 50 μ g/L	K _d [L/kg] at C _w = 10 μ g/L
Batch-derived input parameters (from sorption isotherms and kinetic fit)								
ATZ	402.2	0.464	0.5552	2.156	15.4893	-	49000	117000
IMI	535.0	0.450	0.5642	2.225	11.2236	-	62000	151000
CLO	429.6	0.422	0.3265	2.369	10.1021	-	45000	114000
Best-fit simulations of column data: inhibited BC+Sand								
ATZ	263.3	0.6013	1.9679	1.663	28.2160	1.2168e-07	55000	105000
IMI	439.6	0.5102	0.9873	1.960	21.2937	8.3175e-08	65000	142000
CLO	287.2	0.5562	1.1558	1.798	23.5926	8.2505e-08	51000	103000
Best-fit simulations of column data: biotic BC+Sand								
ATZ	1519	0.4022	0.9847	2.4861	25.1389	1.3027e-07	147000	384000
IMI	1499	0.4170	1.0545	2.3983	17.8317	7.0867e-08	153000	392000
CLO	892.0	0.4565	1.0401	2.1904	19.8953	3.4946e-08	106000	255000

Estimation of Biodegradation Rate

To estimate the biodegradation rate (k_{deg}) for the biotic BC+Sand data set, we used the sorption (K_f , n) and kinetic parameters (τ) derived from the best-fit to the inhibited BC+Sand column data and let the transport model fit k_{deg} by minimizing the sum of squared residuals (SSR). As can be taken from Figure S20, the way the transport model handles biodegradation (as a simple first-order rate only affecting the pesticide concentration in the aqueous phase) was not suitable to adequately describe our biotic BC+Sand column data set. The expansion of the existing transport model with mechanisms to account for biotransformation in all its possible forms was not feasible within the current study. For this reason, as described in the manuscript, we decided to *assume* that for our modelling purposes, the observed mass removal difference between biotic and inhibited BC+Sand columns was due to biologically enhanced sorption only (in order to be conservative and not overestimate the contribution of biodegradation in the subsequent scenario modelling).

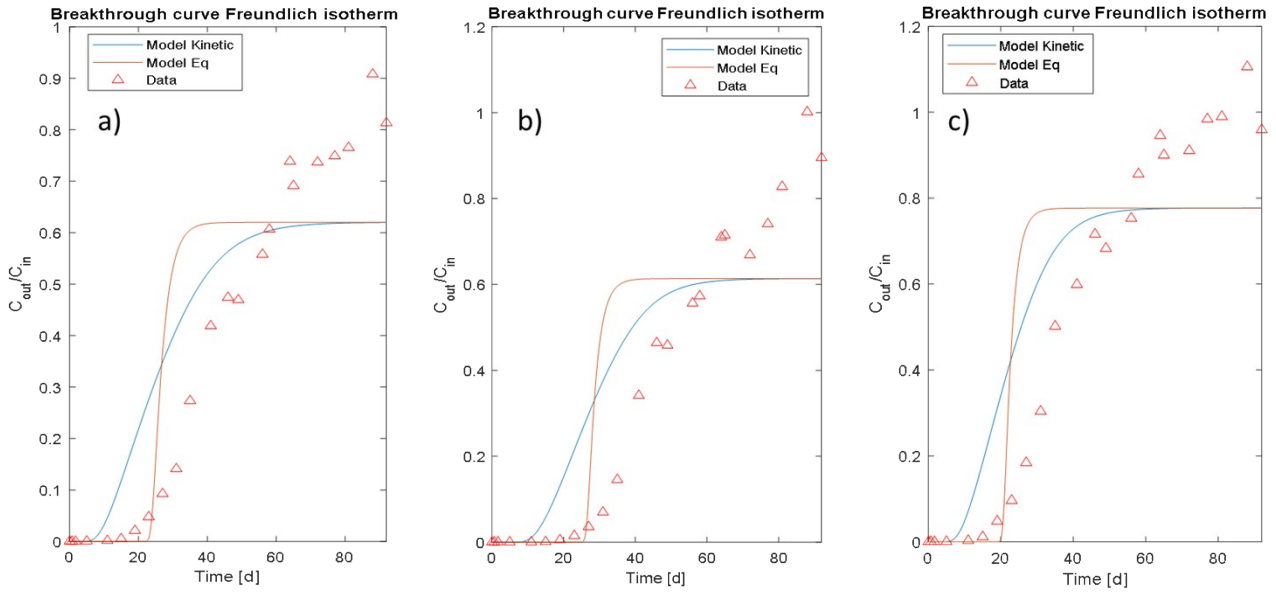


Figure S20: Estimation of first-order biodegradation rate (k_{deg}) for biotic BC+Sand column breakthrough curves using the transport model in MATLAB and assuming Freundlich non-linear sorption behavior. Input values for the sorption and kinetic parameters were taken from the best-fit shown in Figure S18 (best-fit to inhibited BC+Sand data). a) Atrazine, b) imidacloprid, c) clothianidin.

Biofilter Lifetime Simulations (Scenarios)

Table S11: Calculations to adjust simulated continuous filter lifetimes based on a representative field-scale biofilter (infiltration basin) for a residential area of 3 acres and 16 inches per year of average annual rainfall in Denver, CO.

Column Experiment				
Variable	Formula	Parameter	Value	Comments
Diameter		D [cm]	2.5	Measured
Length		L [cm]	5.6	Measured
Area (cross section)	$A = (D/2)^2 * \pi$	A [cm ²]	4.91	
Total porous media volume	$V = A * h$	V [cm ³]	27.49	
Pore volume (BC+Sand)	$PV = V * n$	PV [cm ³]	9.62	~10 mL
Flow rate		Q [ml/min]	0.2114	Measured
		Q [L/year]	111.1	Total volume treated assuming continuous flow
Darcy velocity (infiltration rate)	$q = Q/A$	q [cm/min]	0.04	
		q [cm/h]	2.58	Ulrich: "Linear velocity", 2.6

				cm/h
Porosity (BC+Sand)		n [-]	0.35	Ulrich et al. 2017
Linear pore velocity (BC+Sand)	$v = q/n$	v [cm/min]	0.12	
Case Study				
Variable	Formula	Parameter	Value	Comments
Catchment size (residential)		A_{catch} [acres]	3	Ulrich et al. 2015
Area of infiltration basin (biofilter)		A_{IB} [ft ²]	1112	Ulrich et al. 2015, per recommendation of Denver Urban Drainage and Flood Control District
		A_{IB} [m ²]	103.3	
Denver annual precipitation		P_{annual} [in]	16	Ulrich et al. 2015
		P_{annual} [cm]	40.64	
Total precipitation volume		$V_{\text{precip,annual}}$ [acre-ft]	4	Ulrich et al. 2015
Treatment volume (assume 50%)		$V_{\text{treat,annual}}$ [acre-ft]	2	Ulrich et al. 2015
		$V_{\text{treat,annual}}$ [L]	2.47E+06	
Biofilter Lifetime Adjustment				
Variable	Formula	Parameter	Value	Comments
Area ratio (biofilter/columns)	A_{IB}/A	Area ratio [-]	210456	
Treatment volume columns	$V_{\text{treat,annual}} / \text{Area ratio}$	$V_{\text{treat,annual,columns}}$ [L]	11.72	
Biofilter lifetime adjustment factor	$Q/V_{\text{treat,annual,columns}}$	Factor [-]	9.5	To account for the filter not running continuously.

References

J. D. Berset, S. Mermer, A. E. Robel, V. M. Walton, M. L. Chien and J. A. Field, Direct residue analysis of systemic insecticides and some of their relevant metabolites in wines by liquid chromatography – mass spectrometry, *Journal of Chromatography A*, 2017, **1506**, 45–54.

- R. A. Dick, D. B. Kanne and J. E. Casida, Substrate Specificity of Rabbit Aldehyde Oxidase for Nitroguanidine and Nitromethylene Neonicotinoid Insecticides, *Chem. Res. Toxicol.*, 2006, **19**, 38–43.
- H. Fang, L. Cai, Y. Yang, F. Ju, X. Li, Y. Yu and T. Zhang, Metagenomic analysis reveals potential biodegradation pathways of persistent pesticides in freshwater and marine sediments, *Science of The Total Environment*, 2014, **470–471**, 983–992.
- B. Giroud, A. Vauchez, E. Vulliet, L. Wiest and A. Buleté, Trace level determination of pyrethroid and neonicotinoid insecticides in beebread using acetonitrile-based extraction followed by analysis with ultra-high-performance liquid chromatography–tandem mass spectrometry, *Journal of Chromatography A*, 2013, **1316**, 53–61.
- C. Hao, M. R. Noestheden, X. Zhao and D. Morse, Liquid chromatography–tandem mass spectrometry analysis of neonicotinoid pesticides and 6-chloronicotinic acid in environmental water with direct aqueous injection, *Analytica Chimica Acta*, 2016, **925**, 43–50.
- S. Hussain, C. J. Hartley, M. Shettigar and G. Pandey, Bacterial biodegradation of neonicotinoid pesticides in soil and water systems, *FEMS microbiology letters*.
- B. M. Kim, J.-S. Park, J.-H. Choi, A. M. Abd El-Aty, T. W. Na and J.-H. Shim, Residual determination of clothianidin and its metabolites in three minor crops via tandem mass spectrometry, *Food Chemistry*, 2012, **131**, 1546–1551.
- P. D. Kolekar, S. S. Phugare and J. P. Jadhav, Biodegradation of atrazine by *Rhodococcus* sp. BCH2 to N-isopropylammelide with subsequent assessment of toxicity of biodegraded metabolites, *Environmental Science and Pollution Research*, 2014, **21**, 2334–2345.
- T. Mori, J. Wang, Y. Tanaka, K. Nagai, H. Kawagishi and H. Hirai, Bioremediation of the neonicotinoid insecticide clothianidin by the white-rot fungus *Phanerochaete sordida*, *Journal of Hazardous Materials*, 2017, **321**, 586–590.
- A. MUDHOO and V. K. GARG, Sorption, Transport and Transformation of Atrazine in Soils, Minerals and Composts: A Review, *Pedosphere*, 2011, **21**, 11–25.
- G. Pandey, S. J. Dorrian, R. J. Russell and J. G. Oakeshott, Biotransformation of the neonicotinoid insecticides imidacloprid and thiamethoxam by *Pseudomonas* sp. 1G, *Biochemical and Biophysical Research Communications*, 2009, **380**, 710–714.
- R. Raina-Fulton and A. Behdarvandan, Liquid Chromatography-mass spectrometry for the determination of neonicotinoid insecticides and their metabolites in biological, environmental and food commodity matrices, *Trends Chromatogr*, 2016, **10**, 51–79.
- S. Sagarkar, S. Mukherjee, A. Nousiainen, K. Björklöf, H. J. Purohit, K. S. Jørgensen and A. Kapley, Monitoring bioremediation of atrazine in soil microcosms using molecular tools, *Environmental Pollution*, 2013, **172**, 108–115.
- L. Sánchez-Hernández, D. Hernández-Domínguez, M. T. Martín, M. J. Nozal, M. Higes and J. L. Bernal Yagüe, Residues of neonicotinoids and their metabolites in honey and pollen from sunflower and maize seed dressing crops, *Journal of Chromatography A*, 2016, **1428**, 220–227.
- D. A. Schulz-Jander, W. M. Leimkuehler and J. E. Casida, Neonicotinoid Insecticides: Reduction and Cleavage of Imidacloprid Nitroimine Substituent by Liver Microsomal and Cytosolic Enzymes, *Chem. Res. Toxicol.*, 2002, **15**, 1158–1165.
- E. L. Schymanski, J. Jeon, R. Gulde, K. Fenner, M. Ruff, H. P. Singer and J. Hollender, Identifying Small Molecules via High Resolution Mass Spectrometry: Communicating Confidence, *Environmental Science & Technology*, 2014, **48**, 2097–2098.

- S. Sharma, B. Singh and V. K. Gupta, Assessment of imidacloprid degradation by soil-isolated *Bacillus alkalinitrilicus*, *Environmental Monitoring and Assessment*, 2014, **186**, 7183–7193.
- T. Sharma, A. Rajor and A. P. Toor, Potential of *Enterobacter* sp. Strain ATA1 on imidacloprid degradation in soil microcosm: Effects of various parameters, *Environmental Progress & Sustainable Energy*, 2015, **34**, 1291–1297.
- A. K. Singh and S. S. Cameotra, Influence of microbial and synthetic surfactant on the biodegradation of atrazine, *Environmental Science and Pollution Research*, 2014, **21**, 2088–2097.
- S. Singh, V. Kumar, A. Chauhan, S. Datta, A. B. Wani, N. Singh and J. Singh, Toxicity, degradation and analysis of the herbicide atrazine, *Environmental Chemistry Letters*, 2018, **16**, 211–237.
- B. A. Ulrich, E. A. Im, D. Werner and C. P. Higgins, Biochar and Activated Carbon for Enhanced Trace Organic Contaminant Retention in Stormwater Infiltration Systems, *Environmental Science & Technology*, 2015, **49**, 6222–6230.
- B. A. Ulrich, M. Vignola, K. Edgehouse, D. Werner and C. P. Higgins, Organic Carbon Amendments for Enhanced Biological Attenuation of Trace Organic Contaminants in Biochar-Amended Stormwater Biofilters, *Environmental Science & Technology*, 2017, **51**, 9184–9193.
- T. Van der Velde-Koerts, P. H. Van Hoven-Arentzen and C. M. Mahieu, *Clothianidin (238). Pesticide Residues in Food 2010: Evaluations Part I-Residues; FAO Plant Production and Protection Paper 206.*, World Health Organization & Food and Agriculture Organization of the United States, Rome, 2011.
- W. Xie, C. Han, Y. Qian, H. Ding, X. Chen and J. Xi, Determination of neonicotinoid pesticides residues in agricultural samples by solid-phase extraction combined with liquid chromatography–tandem mass spectrometry, *Journal of Chromatography A*, 2011, **1218**, 4426–4433.
- P. Zhang, C. Ren, H. Sun and L. Min, Sorption, desorption and degradation of neonicotinoids in four agricultural soils and their effects on soil microorganisms, *Science of The Total Environment*, 2018, **615**, 59–69.